The Basic Equations under Weak Temperature Gradient Balance: Formulation, Scaling, and Types of Convectively Coupled Motions

ÁNGEL F. ADAMES[a]

[a] *Department of Atmospheric and Oceanic Sciences, University of Wisconsin–Madison, Madison, Wisconsin*

(Manuscript received 11 August 2021, in final form 25 March 2022)

ABSTRACT: The weak temperature gradient (WTG) approximation is extended to the basic equations on a rotating plane. The circulation is decomposed into a diabatic component that satisfies WTG balance exactly and a deviation from this balance. Scale analysis of the decomposed basic equations reveals a spectrum of motions, including unbalanced inertio-gravity waves and several systems that are in approximate WTG balance. The balanced systems include equatorial moisture modes with features reminiscent of the MJO, off-equatorial moisture modes that resemble tropical depression disturbances, "mixed systems" in which temperature and moisture play comparable roles in their thermodynamics, and moist quasigeostrophic motions. In the balanced systems the deviation from WTG balance is quasi nondivergent, in nonlinear balance, and evolves in accordance to the vorticity equation. The evolution of the strictly balanced WTG circulation is in turn described by the divergence equation. WTG balance restricts the flow to evolve in the horizontal plane by making the isobars impermeable to vorticity and divergence, even in the presence of diabatically driven vertical motions. The vorticity and divergence equations form a closed system of equations when the irrotational circulation is in WTG balance and the nondivergent circulation is in nonlinear balance. The resulting "WTG equations" may elucidate how interactions between diabatic processes and the horizontal circulation shape slowly evolving tropical motions.

SIGNIFICANCE STATEMENT: Many gaps in our understanding of tropical weather systems still exist and there are still many opportunities to improve their forecasting. We seek to further our understanding of the tropics by extending a framework known as the "weak temperature gradient approximation" to all of the equations for atmospheric flow. Doing this reveals a variety of motions whose scales are similar to observed tropical weather systems. We also show that two equations describe the evolution of slow systems: one that describes tropical thunderstorms and one for the rotating horizontal winds. The two equations may help us understand the dynamics of slowly evolving tropical systems.

KEYWORDS: Conservation equations; Dynamics; Moisture/moisture budget; Temperature; Thermodynamics; Tropical variability

1. Introduction

The tropical free troposphere is characterized by a horizontally homogeneous distribution of temperature that varies little with time (Charney 1963; Sobel and Bretherton 2000). This homogeneity is the result of a gravity wave–driven horizontal redistribution of temperature away from precipitating regions, a process referred to as gravity wave adjustment or "buoyant equalization"[1] (Bretherton and Smolarkiewicz 1989; Wolding et al. 2016). As a result of this process the dominant thermodynamic balance in much of the tropics is between adiabatic cooling driven by vertical dry static energy (DSE; s) advection and diabatic heating (Q):

$$\omega \frac{\partial s}{\partial p} \simeq Q, \tag{1}$$

which is the backbone of the "weak temperature gradient" (WTG) approximation (Sobel and Bretherton 2000; Sobel et al. 2001).

The application of the WTG approximation to tropical motions has led to numerous insights on the nature of tropical circulations. It has been applied to understand the Walker cell (Bretherton and Sobel 2002), the diurnal cycle of convection (Ruppert and Hohenegger 2018), convective self-aggregation (Sessions et al. 2010; Holloway and Woolnough 2016), tropical cyclone (TC) formation (Raymond and Sessions 2007; Raymond et al. 2007), and the Madden–Julian oscillation (MJO) (Chikira 2014; Wolding et al. 2016; Janiga and Zhang 2016; Adames et al. 2021). Additionally, the WTG approximation has been used to parameterize the large-scale environment in cloud-permitting models (Raymond and Zeng 2005; Herman and Raymond 2014). These simulations have elucidated how tropical deep convection responds to large-scale

[1] It is not the temperature that gravity waves smooth out, but the virtual temperature, which is more closely related to parcel buoyancy in a moist atmosphere. Most of the free troposphere is dry enough in our current climate that the virtual temperature can be approximated as the temperature. However, their difference becomes large enough that this approximation becomes questionable in a warmer climate (Seidel and Yang 2020).

Supplemental information related to this paper is available at the Journals Online website: https://doi.org/10.1175/JAS-D-21-0215.s1.

Corresponding author: Ángel F. Adames, angel.adamescorraliza@wisc.edu

DOI: 10.1175/JAS-D-21-0215.1

forcing (i.e., horizontal scales much larger than the convection itself), the large-scale thermodynamic environment (Daleu et al. 2015), SST fluctuations (Wang and Sobel 2011), its interaction with the MJO (Wang et al. 2013, 2016), and the impact of the quasi-biennial oscillation on MJO convection (Martin et al. 2019).

A consequence of the WTG approximation is that it allows quasi-balanced circulations to be ubiquitous in the tropics. In this study quasi balance refers to the approximately nondivergent circulations that arise from a balance of processes in one or more of the basic equations. Because of the weaker Coriolis force most of the quasi-balanced circulations are not geostrophic. Rather, they satisfy the more general "nonlinear balance" equation (Bolin 1955; Charney 1955), written in isobaric coordinates as

$$\nabla_h^2\Phi - f\zeta + u\beta - 2\left(\frac{\partial u}{\partial x}\frac{\partial v}{\partial y} - \frac{\partial u}{\partial y}\frac{\partial v}{\partial x}\right) = 0, \tag{2}$$

where Φ is the geopotential, $\zeta = \partial_y v - \partial_x u$ is the relative vorticity, f is the planetary vorticity, and $\beta = df/dy$ is its gradient. This equation can be interpreted as a balance between the divergences of the pressure gradient force, the Coriolis force, and the horizontal momentum advection. Well-known balances such as gradient wind and cyclostrophic balance are special cases of the nonlinear balance equation, and geostrophic balance emerges when the term in parenthesis is negligibly small.

Charney (1963) noted that nonlinear balance occurs in tropical circulations that are outside of regions of deep convection. Held and Hoskins (1985) considered the case of tropical stationary waves that are forced by a prescribed heat source. They found that these circulations are also balanced, although the planetary scale of these waves allowed them to be in geostrophic balance. Balanced circulations in the tropics exist even when diabatic heating is allowed to evolve in time. Sobel et al. (2001) found that balanced moisture waves exist under the WTG approximation that can propagate via horizontal moisture advection. In a toy model where rainfall was made highly sensitive to moisture, Raymond (2001) also found slowly evolving motions with quasi-balanced horizontal winds, as in the moisture waves of Sobel et al. (2001). The type of motions described in these two studies are now referred to as moisture modes, a name that was coined in studies by Yu and Neelin (1994) and Fuchs and Raymond (2002). There is increasing recognition that the MJO has properties of moisture modes, and other tropical motions may as well (Raymond and Fuchs 2009; Sobel and Maloney 2013; Gonzalez and Jiang 2019; Fuchs-Stone et al. 2019; Wolding et al. 2020; Adames and Maloney 2021; Mayta et al. 2022). The existence of slowly evolving, balanced waves under conditions of WTG balance has also been documented in studies by Browning et al. (2000) and Majda and Klein (2003).

Outside of moisture modes, balanced circulations can still play a significant role in the occurrence, intensity, and morphology of tropical convection. In TCs they are responsible for the bulk of the surface heat fluxes that maintain their secondary overturning circulations (Emanuel 1986), and can also induce convergence through cooperative intensification process (Ooyama 1982). In systems that undergo tropical cyclogenesis, the temperature anomalies associated with the balanced flow can modify the thermodynamic environment such that it can change the profiles of ascent in convection (Raymond and Herman 2011; Gjorgjievska and Raymond 2014; Sessions et al. 2015). This modification may also be relevant to large-scale equatorial waves (Kuang 2011). A more recent study by Sessions et al. (2019) showed evidence that convection occurring near the equator may be modulated by balanced dynamics, although possibly in different ways than how it does in systems that undergo tropical cyclogenesis. As their study outlines, understanding how balanced dynamics interacts with convection is important since a better understanding of these may improve the prediction of tropical convection.

The goal of this study is to further understand the motions that occur under the WTG approximation, and how their balanced circulations can interact with deep convection. To do this, we will modify the basic equations by separating the wind field into a diabatic component that satisfies WTG balance exactly and a component that deviates from this exact balance. On the basis of scale analysis, we elucidate the types of convectively coupled weather systems that that may exist in the tropics, many which are in WTG balance. In the slowest of these systems, the basic equations can be reduced to two: one for the irrotational WTG circulation, and one for the nondivergent deviation from exact WTG balance.

This study is structured as follows. Section 2 discusses the form of the basic equations that will be used in this study. In section 3, we decompose the wind field into strict WTG and deviation components and rewrite the basic equations using these definitions. Scale analysis is performed on the recast basic equations in section 4. Section 5 discusses the types of convectively coupled motions that arise from this scaling. The results of the scale analysis is used to simplify the basic equations in section 6. A concluding discussion is shown in section 7.

2. Basic equations

We will begin our analysis by stating the basic equations as applied to the free troposphere. For reference, the main variables and their definitions are shown in Table 1. Because temperature (T), geopotential (Φ), and DSE ($s = C_pT + \Phi$) fluctuations will be central to this study, it will be useful to decompose these fields into a component that satisfies global hydrostatic balance (denoted by the subscript 0) and a component that varies in space and time, denoted by a prime:

$$\Phi(x,y,p,t) = \Phi_0(p) + \Phi'(x,y,p,t), \tag{3a}$$

$$T(x,y,p,t) = T_0(p) + T'(x,y,p,t), \tag{3b}$$

$$s(x,y,p,t) = s_0(p) + s'(x,y,p,t). \tag{3c}$$

With this decomposition, the equations for horizontal momentum, mass continuity, hydrostatic balance, thermodynamic

TABLE 1. The main variables and definitions used in this study.

Variable	Description	Units
$(\cdot)_w$	Component in strict WTG balance	—
$(\cdot)'$	Deviation from strict WTG balance	—
$\mathbf{u}$	Vector wind ($u\mathbf{i} + v\mathbf{j} + \omega\mathbf{j}$)	m s^{-1}
$\mathbf{v}$	Horizontal vector wind ($u\mathbf{i} + v\mathbf{j}$)	m s^{-1}
ω	Vertical velocity	Pa s^{-1}
Φ	Geopotential	m^2 s^{-2}
T	Temperature	K
s	Dry static energy (DSE)	J kg^{-1}
S_p	Vertical DSE gradient ($-\partial_p s$)	J kg^{-1} Pa^{-1}
q	Specific humidity	—
m	Moist static energy (MSE)	J kg^{-1}
Q	Diabatic heating rate	J kg^{-1} s^{-1}
Q_q	Apparent moisture sink	J kg^{-1} s^{-1}
Q_c	Convective heating	J kg^{-1} s^{-1}
Q_r	Radiative heating	J kg^{-1} s^{-1}
F_m	Turbulent MSE flux	Pa J kg^{-1} s^{-1}
δ	Horizontal divergence	s^{-1}
ζ	Vertical relative vorticity	s^{-1}
f	Planetary vorticity	s^{-1}
ζ_a	Vertical absolute vorticity	s^{-1}
$\boldsymbol{\eta}_a$	Vector absolute vorticity	
PV	Potential vorticity	J m^2 kg^{-2} s^{-1}
$\mathbf{J}$	PV forcing vector	J m^3 kg^{-2} s^{-2}
Σ	Deviation from nonlinear balance	s^{-2}
ψ	Streamfunction	m^2 s^{-1}
χ	Velocity potential	m^2 s^{-1}
X	Integrated velocity potential	Pa m^2 s^{-1}
$\mathbf{A}$	Anisotropy between ψ' and χ_w	s^{-1}

energy, and moisture continuity on a tangent plane in isobaric coordinates are written as

$$\frac{D\mathbf{v}}{Dt} = -f\mathbf{k}\times\mathbf{v} - \boldsymbol{\nabla}_h\Phi', \tag{4a}$$

$$\boldsymbol{\nabla}\cdot\mathbf{u} = 0, \tag{4b}$$

$$\frac{\partial\Phi'}{\partial p} = -\frac{R_d T'}{p}, \tag{4c}$$

$$C_p\frac{D_h T'}{Dt} = \omega S_p + Q, \tag{4d}$$

$$\frac{DLq}{Dt} = -Q_q, \tag{4e}$$

where $\mathbf{u} = u\mathbf{i} + v\mathbf{j} + \omega\mathbf{k}$ is the vector wind field, $\mathbf{v} = u\mathbf{i} + v\mathbf{j}$ is the horizontal vector wind, ω is the vertical velocity in isobaric coordinates, f is the planetary vorticity, q is the specific humidity, Q is the diabatic heating rate, Q_q is the apparent moisture sink,

$$S_p = -\frac{\partial s}{\partial p} \tag{4f}$$

is the static stability, defined so it is a positive quantity,

$$\frac{D}{Dt} = \frac{\partial}{\partial t} + \mathbf{u}\cdot\boldsymbol{\nabla}, \quad \frac{D_h}{Dt} = \frac{\partial}{\partial t} + \mathbf{v}\cdot\boldsymbol{\nabla}_h \tag{4g}$$

are the total and horizontal material derivatives in isobaric coordinates, and

$$\boldsymbol{\nabla} \equiv \mathbf{i}\frac{\partial}{\partial x} + \mathbf{j}\frac{\partial}{\partial y} + \mathbf{k}\frac{\partial}{\partial p}, \quad \boldsymbol{\nabla}_h \equiv \mathbf{i}\frac{\partial}{\partial x} + \mathbf{j}\frac{\partial}{\partial y} \tag{4h}$$

are the gradient operator in isobaric coordinates and the horizontal gradient. The constants in Eq. (1) are the specific heat at constant pressure ($C_p = 1005$ J kg^{-1} K^{-1}), the latent energy of vaporization ($L = 2.5\times10^6$ J kg^{-1}), and the dry gas constant ($R_d = 287$ J kg^{-1} K^{-1}).

Note that in defining the terms in Eq. (4) we are assuming that deviations from global hydrostatic balance are also hydrostatic. We also note that while ignoring free tropospheric friction simplifies our analysis, its neglection is a caveat of this study since it can be important for equatorial low-frequency oscillations (Kim and Zhang 2021).

To better understand motion under the WTG approximation, it will be convenient to consider the vorticity and divergence equations. The vorticity equation is obtained by taking the curl of Eq. (4a) and retaining only the vertical component. The divergence equation is obtained by taking the horizontal divergence of Eq. (4a). The pair of equations are written as

$$\frac{D\zeta}{Dt} = -v\beta - \zeta_a\delta + \mathbf{k}\cdot\left(\frac{\partial\mathbf{v}}{\partial p}\times\boldsymbol{\nabla}_h\omega\right), \tag{5}$$

$$\frac{D\delta}{Dt} = -\Sigma - \frac{\partial\mathbf{u}}{\partial p}\cdot\boldsymbol{\nabla}\omega, \tag{6}$$

where $\delta = \partial_x u + \partial_y v$ is the horizontal divergence, $\zeta_a = \zeta + f$ is the vertical component of the absolute vorticity, and

$$\Sigma \equiv \nabla_h^2\Phi' - f\zeta + u\beta - 2\mathbf{k}\cdot(\boldsymbol{\nabla}_h u\times\boldsymbol{\nabla}_h v) \tag{7}$$

will be referred to as the deviation from nonlinear balance, noting that the terms on the rhs are those shown in Eq. (2). In Raymond (1992) the symbol Σ is used to denote the deviation from geostrophic balance. We are keeping the same symbol but noting that it is for a different definition.

We will make use of the DSE budget, which is obtained from Eq. (4d) if we assume that the Lagrangian derivative of Φ is dominated by its vertical advection:

$$\frac{D\Phi}{Dt} \simeq \omega\frac{\partial\Phi}{\partial p} \tag{8}$$

and then used to write the thermodynamic equation as

$$\frac{Ds}{Dt} \simeq Q. \tag{9}$$

We will use this budget since the MSE budget, which is just the DSE budget with Eq. (4e) added to it, is widely used and because using the DSE budget only adds small errors when compared to simply using Eq. (4d) (Sobel et al. 2014). For completeness, we show in SI section 1 that the same results can be obtained if the potential temperature budget is used as our thermodynamic equation.

The diabatic heating rate Q is composed of contributions from microphysical processes, radiative heating Q_r, and turbulent fluxes of DSE (F_s)

$$Q \equiv Q_c + Q_r, \tag{10}$$

where

$$Q_c \equiv L(c - e) - \frac{\partial F_s}{\partial p} \tag{11}$$

is the convective heating, where c and e are the condensation and evaporation rates, respectively. The moisture sink Q_q is composed of a contribution from microphysical processes and turbulent fluxes of moisture (F_{Lq}):

$$Q_q \equiv L(c - e) + \frac{\partial F_{Lq}}{\partial p}. \tag{12}$$

As mentioned previously, the MSE budget can be obtained by adding Eqs. (13) and (4e), yielding

$$\frac{Dm}{Dt} \simeq Q_r - \frac{\partial F_m}{\partial p}, \tag{13}$$

where $m = s + Lq$ is the MSE and $F_m = F_s + F_{Lq}$ is the eddy flux of MSE.

Interesting interpretations about the processes that drive rotation in the tropics can be obtained by examining the Ertel potential vorticity (PV). Here we define the PV using DSE rather than potential temperature:

$$\text{PV} = -g\boldsymbol{\eta}_a \cdot \boldsymbol{\nabla} s, \tag{14a}$$

where

$$\boldsymbol{\eta}_a = -\frac{\partial v}{\partial p}\mathbf{i} + \frac{\partial u}{\partial p}\mathbf{j} + \zeta_a \mathbf{k} \tag{14b}$$

is the absolute vorticity vector. For most large-scale motions on Earth the PV is largely determined by its vertical contribution:

$$\text{PV} \simeq g\zeta_a S_p. \tag{15}$$

In an inviscid atmosphere, the PV budget is written as

$$\frac{D\text{PV}}{Dt} = -g\boldsymbol{\eta}_a \cdot \boldsymbol{\nabla} Q. \tag{16}$$

It is worth pointing out that when deriving a DSE-based PV the DSE gradient does not fully annihilate the solenoidal term in the vorticity equation [see derivations in Schubert et al. (2001) and Vallis (2017)]. However, we found that this contribution is negligibly small (not shown).

3. Decomposing the winds into exact WTG and deviation components

a. The WTG balanced circulation

While the WTG approximation is usually defined as Eq. (1), it will be convenient to write it as

$$\mathbf{u} \cdot \boldsymbol{\nabla} s \simeq Q. \tag{17}$$

This is the same definition of WTG balance that is employed in studies of column-integrated DSE budgets (Inoue and Back 2015, 2017; Inoue et al. 2021), and is approximately equal to Eq. (1) in much of the tropical free troposphere. Using Eq. (17) rather than Eq. (1) allows us to more clearly separate the strict WTG component of the flow and its deviation. It will also show more clearly how the WTG balanced circulation modulates PV.

We decompose the total wind field into a component that satisfies WTG balance exactly (denoted by the subscript w) and a component that deviates from this exact balance (denoted by a prime)

$$\mathbf{u} = \mathbf{u}_w + \mathbf{u}', \tag{18a}$$

$$\mathbf{u}_w \cdot \boldsymbol{\nabla} s \equiv Q. \tag{18b}$$

The WTG-balanced circulation $\mathbf{u}_w$ is further decomposed into convective ($\mathbf{u}_c$) and radiative ($\mathbf{u}_r$) contributions:

$$\mathbf{u}_w \equiv \mathbf{u}_c + \mathbf{u}_r, \tag{19a}$$

$$\mathbf{u}_c \cdot \boldsymbol{\nabla} s \equiv Q_c, \tag{19b}$$

$$\mathbf{u}_r \cdot \boldsymbol{\nabla} s \equiv Q_r. \tag{19c}$$

Since $\mathbf{u}_w$ satisfies WTG balance exactly, it follows that the horizontal circulation ($\mathbf{v}_w$) is irrotational and is related to the vertical motion (ω_w) through mass continuity. As a result, we can define $\mathbf{v}_w$ in terms of a WTG velocity potential (χ_w):

$$\mathbf{v}_w = \boldsymbol{\nabla}_h \chi_w, \tag{20a}$$

which we use to write the WTG mass continuity equation as

$$\frac{\partial \omega_w}{\partial p} = -\delta_w = -\nabla_h^2 \chi_w. \tag{20b}$$

Equations (20a) and (20b) indicate that only one variable is needed to describe the distribution of $\mathbf{u}_w$. We show this by following Lorenz (1960) and Raymond (1992) and defining the integrated velocity potential:

$$X_w(x, y, p, t) \equiv \int_0^p \chi_w(x, y, p', t) dp'. \tag{20c}$$

By defining X_w we can write Eq. (18b) as

$$\left(\frac{\partial s'}{\partial x}\frac{\partial^2}{\partial x \partial p} + \frac{\partial s'}{\partial y}\frac{\partial^2}{\partial y \partial p} + S_p \nabla_h^2\right) X_w = Q. \tag{20d}$$

All components of $\mathbf{u}_w$ can be obtained by solving Eq. (20d) for X_w.

By defining a component of the wind field that satisfies WTG balance exactly, we can simplify Eq. (13) to the following:

$$\frac{\partial s}{\partial t} = -\mathbf{u}' \cdot \boldsymbol{\nabla} s. \tag{21}$$

Equation (21) shows that only deviations from strict WTG balance can induce a DSE tendency.

Unlike $\mathbf{v}_w$, $\mathbf{v}'$ is composed of both irrotational and nondivergent contributions:

$$\mathbf{v}' = \mathbf{k} \times \nabla_h \psi' + \nabla_h \chi', \tag{22}$$

where ψ' is the streamfunction and χ' is the velocity potential that deviates from strict WTG balance. As in the strict WTG component of the circulation, χ' and ω' are related through mass continuity:

$$\frac{\partial \omega'}{\partial p} = -\delta' = -\nabla_h^2 \chi', \tag{23}$$

while the vorticity can be obtained from the horizontal Laplacian of the streamfunction:

$$\zeta = \nabla_h^2 \psi'. \tag{24}$$

b. Moisture and MSE budgets

We can use Eqs. (18b) and (21) to rewrite Eq. (4e) as

$$\frac{\partial Lq}{\partial t} = -(\mathbf{u}' + \mathbf{u}_r) \cdot \nabla Lq - \mathbf{u}_c \cdot \nabla m - \frac{\partial F_m}{\partial p}. \tag{25}$$

Equation (26) is similar to the WTG moisture equation discussed by Adames et al. (2021), except that it is based on the definitions of WTG balance presented in the previous subsection. With these definitions, we see that $\mathbf{u}'$ and $\mathbf{u}_r$ contribute to the moisture tendency via moisture advection. The convectively driven circulation, however, advects MSE rather than moisture. This difference is due to the loss of moisture from microphysical processes such as condensation, which appear in Eq. (26) as the DSE contribution to the MSE advection.

The MSE budget can be obtained by adding Eqs. (26) and (21), yielding

$$\frac{\partial m}{\partial t} = -\mathbf{u}_r \cdot \nabla Lq - (\mathbf{u}' + \mathbf{u}_c) \cdot \nabla m - \frac{\partial F_m}{\partial p}, \tag{26}$$

where we note that the radiatively driven circulation is the only one that modifies the MSE purely through moisture advection, while $\mathbf{u}'$ and $\mathbf{u}_c$ advect MSE.

c. Potential vorticity

As in Haynes and McIntyre (1987), we write the PV budget in terms of a forcing vector $\mathbf{J}$:

$$\frac{\partial \mathrm{PV}}{\partial t} = -\nabla \cdot \mathbf{J}, \tag{27}$$

where

$$\mathbf{J} = \mathbf{u}\mathrm{PV} + g\boldsymbol{\eta}_a Q. \tag{28}$$

The vector $\mathbf{J}$ is composed of two contributions: a PV flux term and a PV generation term. The flux term has contributions from strict WTG balance and its deviation, while the generation term is in strict WTG balance. We can combine the WTG contributions into a single term by using Eqs. (18a) and (18b) and the vector triple product identity, yielding the following expression for $\mathbf{J}$:

$$\mathbf{J} = \mathbf{J}_w + \mathbf{J}', \tag{29a}$$

where

$$\mathbf{J}_w \equiv \nabla s \times (\boldsymbol{\eta}_a \times \mathbf{u}_w) \tag{29b}$$

is the strict WTG component of $\mathbf{J}$, and

$$\mathbf{J}' \equiv \mathbf{u}'\mathrm{PV} \tag{29c}$$

is the contribution from deviations from strict WTG balance.

From examination of Eq. (29b) we can interpret $\mathbf{J}_w$ as the cross product of the Coriolis force that $\mathbf{u}_w$ experiences and the DSE gradient. Isentropic surfaces roughly correspond to pressure surfaces in the tropics, implying that $\mathbf{J}_w$ is quasi horizontal.

To better understand how WTG balance and its departure affect the evolution of PV we invoke the impermeability theorem (Haynes and McIntyre 1987, 1990). Let us consider two concentric spheres that are made out of isentropic surfaces, neither which intersect the ground, as depicted in Fig. 1a (see also Fig. 4.11 of Vallis 2017). The impermeability theorem states that PV cannot be fluxed across the isentropic surfaces and hence the mass-weighted integral between the two isentropes is constant in time (see SI section 2). It follows that $\mathbf{J}_w$ and $\mathbf{J}'$ can modulate the PV in the tropics in the following ways:

1) Diabatic heating in the tropics modulates PV locally by concentrating the PV that lies within the isentropic surfaces while diluting it in other regions of the tropics (Fig. 1b). It does not create it nor destroy it.
2) Vertical motions that arise from departures from strict WTG balance do not flux PV across isentropes. Instead, they concentrate the PV by squeezing or stretching the isentropes in such a way that the mass-weighted integral of PV within the two isentropes remains unchanged (Fig. 1c).
3) If the distribution of PV is not homogeneous within the two isentropic surfaces then PV can be redistributed through horizontal advection.

When considered together, points 1 and 2 imply that there is no net vertical exchange of PV in circulations that are in strict WTG balance. As a result, the movement of PV is quasi horizontal. Only strong departures from WTG balance can cause the PV flux to have a significant vertical component. This can occur in the inertio-gravity waves that adjust the troposphere to WTG balance in the first place, in some planetary-scale waves, or in TCs.

4. Scale analysis

We can obtain some insights to the types of phenomena that can occur in the tropics by using the decomposition from the previous section to perform a scale analysis of Eq. (4). The analysis will largely follow Adames et al. (2019), except it will be generalized to the observed tropical troposphere. The main scales and their definitions are shown in Table 2. The

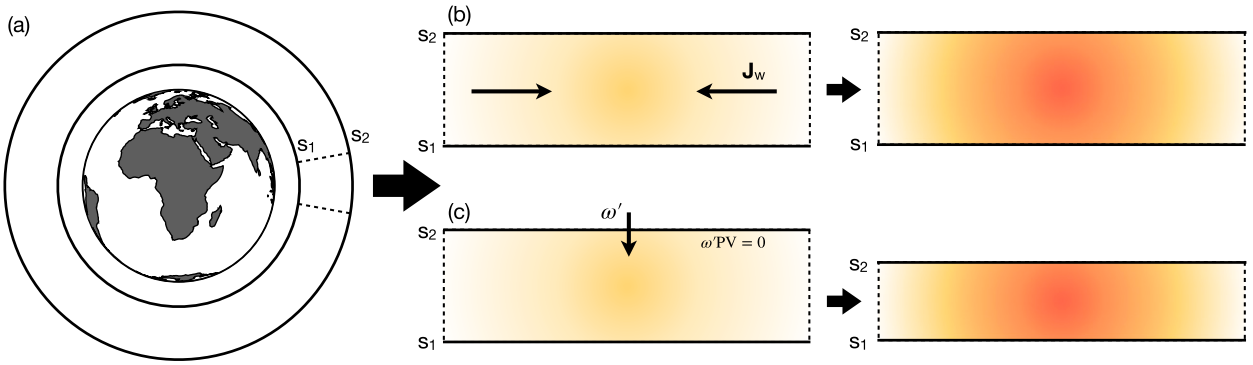

FIG. 1. Schematic describing (a) two concentric isentropic layers that lie above Earth's surface. Two processes that modulate PV within these two layers are (a) horizontal convergence of $\mathbf{J}_w$, which increases the PV concentration at a given location within the concentric spheres, and (b) concentration of the PV by squeezing the isentropic surfaces, a process that is done only by departures from strict WTG balance. The depth of the atmosphere in (a) is exaggerated for the purposes of presentation.

independent variables of this study are nondimensionalized as follows:

$$x = \mathrm{L}_x\hat{x}, \quad y = \mathrm{L}_y\hat{y}, \quad p = \mathrm{P}\hat{p}, \quad t = \tau\hat{t}, \tag{30a}$$

where the capitalized roman letters are dimensional scales and the hats are nondimensional variables. These four scales actually correspond to the inverse of the wavenumber and wave frequency. As a result, it will be useful to also discuss the spatial scale of a system in terms of their wavelength:

$$(\lambda_x, \lambda_y, \lambda_p) = 2\pi(\mathrm{L}_x, \mathrm{L}_y, \mathrm{P}). \tag{30b}$$

TABLE 2. Scales and the equation in which they are defined.

Scale	Description	Defined in
L_x	Zonal scale	(30a)
L_y	Meridional scale	(30a)
L_d	Rossby deformation radius	(46b)
P	Vertical scale	(30a)
τ	Temporal scale	(30a)
U	Zonal wind scale	(30f)
W	Vertical velocity scale	(30f)
q	Specific humidity scale	(30c)
T	Temperature scale	(30c)
ϕ	Geopotential scale	(30c)
c	Gravity wave phase speed scale	(44)
c_p	Phase speed scale	(38)
Q_c	Convective heating scale	(30h)
R	Radiative heating scale	(30i)
S_0	Vertical DSE gradient scale	(30h)
$\mathcal{L}_p$	Vertical latent energy gradient scale	(30h)
Ro_τ	Temporal Rossby number	(35)
Ro	Rossby number	(35)
Bu	Burger number	(46b)
Fr	Froude number	(46c)
Fr_τ	Wave-based Froude number	(46c)
ϵ	Fraction of $\mathbf{v}'$ that is irrotational	(31)
$\hat{\epsilon}$	Vertical velocity scale	(31)
$\hat{\alpha}$	Ratio of $\mathcal{L}_p$ to S_0	(52b)
N_w	Nondimensional WTG balance number	(41)
$\mathrm{N}_{\mathrm{mode}}$	Magnitude of $\mathrm{C}_p\mathrm{T}$ with respect to Lq	(62)

The specific humidity and the perturbation geopotential, temperature, and DSE scale as

$$q = \mathrm{q}\hat{q}, \quad \Phi' = \phi\hat{\Phi}, \quad T' = \mathrm{T}\hat{T}, \quad s' = C_p\mathrm{T}\hat{s}, \tag{30c}$$

while the hydrostatic components are assumed to scale independently, so that the vertical DSE gradient scales as

$$S_p = \mathrm{S}_0\frac{\partial\hat{s}_0}{\partial\hat{p}} + \frac{C_p\mathrm{T}}{\mathrm{P}}\frac{\partial\hat{s}'}{\partial\hat{p}}. \tag{30d}$$

The wind components $\mathbf{u}_w$ and $\mathbf{u}'$ contribute differently to the evolution of DSE and moisture. For these equations, we will scale $\mathbf{u}_w$ and $\mathbf{u}'$ separately:

$$\omega_w = \mathrm{W}_w\hat{\omega}_w, \quad \omega' = \mathrm{W}'\hat{\omega}', \quad u_w = \mathrm{U}_w\hat{u}_w, \quad u' = \mathrm{U}'\hat{u}'. \tag{30e}$$

In the momentum budget, it will be convenient to scale the total horizontal wind since the decomposition of the wind in Eqs. (18a) does not affect its interpretation. For this equation the total wind scale is assumed to be of the same magnitude as the largest of either U_w or U':

$$\mathrm{U} = \max(\mathrm{U}_w, \mathrm{U}'), \quad \mathrm{W} = \max(\mathrm{W}_w, \mathrm{W}'). \tag{30f}$$

For simplicity, we will assume that the scale of the meridional wind (V) is proportional to the scale of the zonal wind multiplied by the aspect ratio of the zonal and meridional scales:

$$\mathrm{V} \sim \frac{\mathrm{L}_y}{\mathrm{L}_x}\mathrm{U}. \tag{30g}$$

The convective heating and the apparent moisture sink will follow the same scaling since they are both related to convective processes:

$$(Q_c, Q_q) = \mathrm{Q}_c(\hat{Q}_c, \hat{Q}_q). \tag{30h}$$

The scaling for the radiative heating is written as

$$Q_r = \mathrm{R}\hat{Q}_r. \tag{30i}$$

Last, we will scale $F_m = \mathrm{F}\hat{F}_m$, completing our set of variables and scales.

a. Mass continuity and horizontal momentum

We will begin our scaling with the continuity equation [Eq. (20c)], separated into contributions from $\mathbf{u}_w$ and $\mathbf{u}'$. We first nondimensionalize Eq. (22) to obtain the following:

$$\hat{\mathbf{v}}' = (1-\epsilon)\hat{\mathbf{v}}'_\psi + \epsilon\hat{\mathbf{v}}'_\chi, \tag{31a}$$

where

$$\epsilon = \frac{\mathrm{U}'_\chi}{\mathrm{U}'} \tag{31b}$$

is a nondimensional scale that describes the relative magnitude between the scales of the irrotational (U'_χ) and total non-WTG winds, similar to the scaling used by Raymond (1992). The nondivergent winds scale as $(1-\epsilon)$ so that $\mathbf{v}'$ is irrotational when $\epsilon \to 1$ and nondivergent when $\epsilon \to 0$.

By considering the nondimensional continuity equations for $\mathbf{u}_w$ and $\mathbf{u}'$ separately we find that

$$\mathrm{W}_w \sim \frac{\mathrm{U}_w \mathrm{P}}{\mathrm{L}_x}, \quad \mathrm{W}' \sim \epsilon\frac{\mathrm{U}'\mathrm{P}}{\mathrm{L}_x}, \tag{32}$$

from which we can define the scale of the total vertical velocity as

$$\mathrm{W} = \hat{\epsilon}\frac{\mathrm{U}\mathrm{P}}{\mathrm{L}_x}\hat{\epsilon} = \max\left(\frac{\mathrm{U}_w}{\mathrm{U}}, \epsilon\frac{\mathrm{U}'}{\mathrm{U}}\right). \tag{33}$$

Replacing the terms in the momentum equation with the scales in Eq. (30), we obtain the following:

$$\mathrm{Ro}_\tau\frac{\partial\hat{u}}{\partial\hat{t}} + \mathrm{Ro}\left(\hat{\mathbf{v}}\cdot\hat{\boldsymbol{\nabla}}\hat{u} + \hat{\epsilon}\hat{\omega}\frac{\partial\hat{u}}{\partial\hat{p}}\right) = \frac{\mathrm{L}_y}{\mathrm{L}_x}\left(\hat{f}\hat{v} - \mathrm{G}\frac{\partial\hat{\Phi}}{\partial x}\right), \tag{34a}$$

$$\frac{\mathrm{L}_y}{\mathrm{L}_x}\left[\mathrm{Ro}_\tau\frac{\partial\hat{v}}{\partial\hat{t}} + \mathrm{Ro}\left(\hat{\mathbf{v}}\cdot\hat{\boldsymbol{\nabla}}\hat{v} + \hat{\epsilon}\hat{\omega}\frac{\partial\hat{u}}{\partial\hat{p}}\right)\right] = -\hat{f}\hat{u} - \mathrm{G}\frac{\partial\hat{\Phi}}{\partial y}, \tag{34b}$$

where

$$\mathrm{Ro} = \frac{\mathrm{U}}{f\mathrm{L}_x}, \quad \mathrm{Ro}_\tau = \frac{1}{f\tau} \tag{35}$$

are the Rossby number and a time-scale-based Rossby number, and

$$\mathrm{G} = \max(1, \mathrm{Ro}_\tau, \mathrm{Ro}) \tag{36}$$

is the scaling for the pressure gradient force, chosen so that it is always a leading-order term. The geopotential can have quasigeostrophic (QG) scaling when $\mathrm{Ro}_\tau < \mathrm{L}_y/\mathrm{L}_x$ or a scaling similar to that of Charney (1963) when $\mathrm{Ro}_\tau \geq \mathrm{L}_y/\mathrm{L}_x$:

$$\phi = \begin{cases} f\mathrm{U}\mathrm{L}_y, & \text{if} \quad \mathrm{Ro}_\tau < \mathrm{L}_y/\mathrm{L}_x, \\ \mathrm{c}_p\mathrm{U}, & \text{if} \quad \mathrm{Ro}_\tau \geq \mathrm{L}_y/\mathrm{L}_x. \end{cases} \tag{37}$$

In most applications of scale analysis, τ is defined as the "advective time scale," so that $\tau = \mathrm{L}_x/\mathrm{U}$, and hence $\mathrm{Ro}_\tau = \mathrm{Ro}$. Instead of making this assumption, we will follow Adames et al. (2019) and assume that τ is governed by wave motion:

$$\tau = \frac{\mathrm{L}_x}{\mathrm{c}_p}, \tag{38}$$

where c_p is the characteristic zonal phase speed of a wave.

b. Vorticity equation

To properly scale Eq. (4), we must obtain an expression for the ratio between U_w and U in terms of other scales. This can be done by examining the nondimensional vorticity equation. The vorticity scales as

$$\zeta \sim (1-\epsilon)\frac{\mathrm{U}'}{\mathrm{L}_y}\hat{\zeta}, \tag{39}$$

recalling that Eq. (20) states that only the deviation from strict WTG balance can have a nonzero vorticity. Following Eq. (30), we write the nondimensional vorticity equation as

$$(1-\epsilon)\frac{\mathrm{L}_y}{\mathrm{L}_x}\left(\mathrm{Ro}_\tau\frac{\partial\hat{\zeta}}{\partial\hat{t}} + \mathrm{Ro}\hat{\mathbf{v}}\cdot\hat{\boldsymbol{\nabla}}_h\hat{\zeta} - \hat{\epsilon}\mathrm{Ro}\hat{\omega}\frac{\partial\hat{\zeta}}{\partial\hat{p}}\right)$$
$$= -\frac{\beta\mathrm{L}_y}{f}\hat{v} - \hat{\epsilon}\left[\frac{\mathrm{L}_x}{\mathrm{L}_y}\mathrm{Ro}(1-\epsilon)\hat{\zeta} + \hat{f}\right]\hat{\delta} + \hat{\epsilon}\mathrm{Ro}\mathbf{k}\cdot\left(\frac{\partial\hat{\mathbf{v}}}{\partial\hat{p}}\times\hat{\boldsymbol{\nabla}}_h\hat{\omega}\right), \tag{40}$$

noting that we have assumed that $\mathrm{U}' \sim \mathrm{U}$. For the case when $\omega = \omega_w$, we have that $\hat{\epsilon} \sim \mathrm{U}_w/\mathrm{U}$. If we assume that vortex stretching is always of leading-order importance in the vorticity equation, the ratio between the non-WTG and WTG winds scales as

$$\frac{\mathrm{U}_w}{\mathrm{U}'} = \min\left[1, \frac{\mathrm{L}_x}{\mathrm{L}_y}\mathrm{Ro}_\tau, \frac{\mathrm{L}_x\mathrm{c}_p}{\mathrm{L}_y\mathrm{U}(1-\epsilon)}\right], \tag{41}$$

indicating that $\mathbf{v}'$ is much larger than $\mathbf{v}_w$ in either QG systems or systems in which $\mathrm{L}_x \sim \mathrm{L}_y$ and $\mathrm{U} \gg \mathrm{c}_p$, such as TCs.

From Eq. (41) we can show that $\hat{\epsilon}$ can be qualitatively written as follows:

$$\hat{\epsilon} \sim \max\left(\frac{\mathrm{U}_w}{\mathrm{U}'}, \epsilon\right). \tag{42}$$

Given that $\epsilon \leq 1$, and that $\mathrm{U}_w/\mathrm{U}' \sim 1$ except for QG systems and TCs, it follows that $\hat{\epsilon} \sim 1$ under most scaling values.

c. Divergence equation

We can use the scales in Eq. (30) to make the divergence equation nondimensional:

$$\hat{\epsilon}\left(\mathrm{Ro}_\tau \frac{\partial \hat{\delta}}{\partial \hat{t}} + \mathrm{Ro}\hat{\mathbf{v}} \cdot \hat{\boldsymbol{\nabla}}_h \hat{\delta} - \hat{\epsilon}\mathrm{Ro}\hat{\omega}\frac{\partial \hat{\delta}}{\partial \hat{p}}\right) = -\hat{\boldsymbol{\nabla}}_h \cdot (\hat{\boldsymbol{\nabla}}_h \mathrm{G}\hat{\Phi} - \hat{f}\hat{\boldsymbol{\nabla}}_h \hat{\psi}') - \hat{\epsilon}^2 \mathrm{Ro}\hat{\delta}^2 + 2\mathrm{Ro}\mathbf{k} \cdot (\hat{\boldsymbol{\nabla}}_h \hat{u} \times \hat{\boldsymbol{\nabla}}_h \hat{v}) - \hat{\epsilon}\mathrm{Ro}\frac{\partial \hat{\mathbf{v}}}{\partial \hat{p}} \cdot \hat{\boldsymbol{\nabla}}_h \hat{\omega}. \quad (43)$$

From examination of Eq. (43) we see that when $(\hat{\epsilon}, \mathrm{Ro}, \mathrm{Ro}_\tau) \ll 1$ the leading-order balance is the definition of geostrophic vorticity. When $\hat{\epsilon} \ll 1$ but $(\mathrm{Ro}, \mathrm{Ro}_\tau) \sim 1$ nonlinear balance prevails (Charney 1955; Raymond 1992). For many types of convectively coupled tropical motions $\hat{\epsilon} \sim 1$ and $(\mathrm{Ro}, \mathrm{Ro}_\tau) \sim 1$ so that no term is negligible in Eq. (43).

d. Hydrostatic and thermodynamic energy scaling

To scale the hydrostatic equation [Eq. (4c)], we define a scale for the phase speed of dry gravity waves as

$$\mathrm{c} \sim \mathrm{P}\left(\frac{R_d \mathrm{S}_0}{p C_p}\right)^{1/2}. \quad (44)$$

Online supplementary information (SI) section 3 shows that this is the actual phase speed of gravity waves in a simplified atmosphere in which the term in parenthesis in Eq. (44) is held constant. If we assume that this term is on the order of $\sim 10^{-5}$ m^2 s^{-2} Pa^{-2}, we obtain a value of c of ~50 m s^{-1} for a gravity wave with a first baroclinic vertical structure (i.e., $\lambda_p \sim 10^5$ Pa, which yields a value of P of $\sim 1.6 \times 10^4$ Pa).

With c defined, we can obtain the following scaling between T and Φ from Eq. (4c):

$$\mathrm{T} \sim \frac{\mathrm{S}_0 \mathrm{P}}{C_p \mathrm{c}^2}\,\phi. \quad (45)$$

We will now nondimensionalize Eqs. (18b) and (21) individually, and later consider the thermodynamic equation as a whole. We begin by obtaining a nondimensional version of Eq. (21) by combining it with Eqs. (32), (37), and (45), yielding the following:

$$\max\left(\mathrm{Fr}_\tau^2, \frac{\mathrm{Fr}_\tau}{\mathrm{Bu}^{1/2}}\right)\left(\frac{\partial \hat{s}'}{\partial \hat{t}} + \frac{\mathrm{Fr}}{\mathrm{Fr}_\tau}\hat{\mathbf{v}}' \cdot \hat{\boldsymbol{\nabla}}_h \hat{s}' + \epsilon \frac{\mathrm{Fr}}{\mathrm{Fr}_\tau}\hat{\omega}'\frac{\partial \hat{s}'}{\partial \hat{p}}\right) + \epsilon \hat{\omega}' \frac{\partial \hat{s}_0}{\partial \hat{p}} = 0, \quad (46a)$$

where

$$\mathrm{Bu} \equiv \left(\frac{\mathrm{L}_d}{\mathrm{L}_y}\right)^2, \quad \mathrm{L}_d = \frac{\mathrm{c}}{f} \quad (46b)$$

is the Burger number, and L_d is the Rossby radius of deformation,

$$\mathrm{Fr} \equiv \frac{\mathrm{U}}{\mathrm{c}}, \quad \mathrm{Fr}_\tau \equiv \frac{\mathrm{c}_p}{\mathrm{c}} \quad (46c)$$

are the conventional and wave-based Froude number, the latter defined as in Adames et al. (2019). The Burger number measures the importance of vertical stratification relative to Earth's rotation. A value of Bu that is much larger than unity implies that the gravity wave adjustment process toward WTG is more important than the geostrophic adjustment process. The number Fr_τ is the ratio of the gravity wave adjustment time scale τ_g to the system's time scale while Fr is the ratio of the advective time scale to τ_g. Both can be considered measures on how quickly the system evolves relative to the adjustment to WTG balance. The Froude and Rossby numbers satisfy the following equivalence:

$$\frac{\mathrm{Fr}}{\mathrm{Fr}_\tau} = \frac{\mathrm{Ro}}{\mathrm{Ro}_\tau} = \frac{\mathrm{U}}{\mathrm{c}_p}, \quad (46d)$$

which can be thought of as the ratio of horizontal DSE advection to the DSE tendency.

For the terms in Eq. (46a) to always be on the same order of magnitude we require that

$$\epsilon = \max\left(\mathrm{Fr}_\tau^2, \frac{\mathrm{Fr}_\tau}{\mathrm{Bu}^{1/2}}\right), \quad (47)$$

so that the deviation from WTG becomes increasingly nondivergent with slower propagation. This equivalence is similar to the scaling found by Raymond (1992). In fact, Eq. (47) becomes identical to his Eq. (16) when $\mathrm{c}_p \sim \mathrm{U}$.

With ϵ defined, we can define the nondimensional static stability as

$$\hat{S}_p = \frac{\partial \hat{s}_0}{\partial \hat{p}} + \epsilon \frac{\mathrm{Fr}}{\mathrm{Fr}_\tau}\frac{\partial \hat{s}'}{\partial \hat{p}}, \quad (48)$$

which reveals that when $\epsilon \ll 1$, temporal variations in S_p are negligible.

We will now obtain a nondimensional version of Eq. (18b). We assume that in regions of heavy precipitation a leading-order balance that is analogous to Eq. (1) exists in Eq. (4e) between vertical moisture advection and the moisture sink:

$$\omega \frac{\partial Lq}{\partial p} \sim -Q_q. \quad (49)$$

This assumption is physically grounded on the fact that in convective regions, loss of moisture from condensation is approximately balanced by the vertical moisture advection from the convection itself (Neelin and Held 1987; Raymond et al. 2009; Adames et al. 2021). In these regions, it is reasonable to assume that $\mathrm{W} \sim \mathrm{W}_w$, and that the vertical latent energy gradient scales as

$$\frac{\partial Lq}{\partial p} \sim \mathcal{L}_p \frac{\partial \hat{q}}{\partial \hat{p}}, \quad (50)$$

where $\mathcal{L}_p$ is a characteristic vertical latent energy gradient. Because vertical moisture advection associated with deep convection tends to be a maximum between the 400- and 700-hPa levels (Benedict and Randall 2007; Wolding et al. 2016), we will use a value of $\mathcal{L}_p$ that is characteristic of this region.

By using the scaling in Eqs. (30) and (49), we obtain the following relationship between convective heating and the convective vertical velocity:

$$\mathrm{Q}_c \sim \mathcal{L}_p \mathrm{W}_w. \quad (51)$$

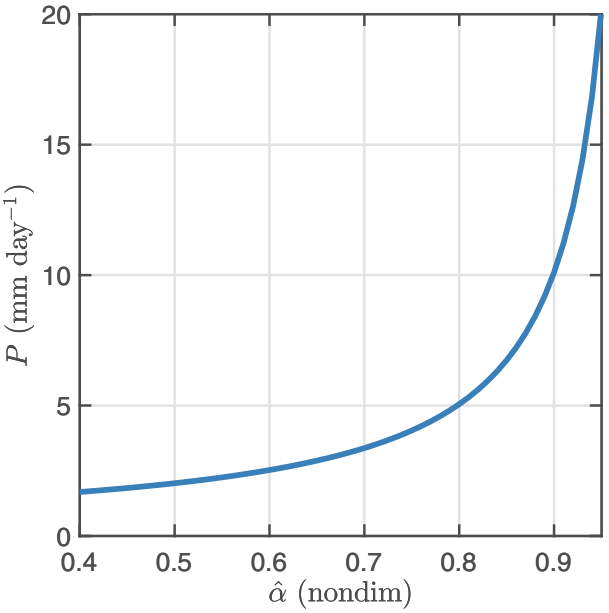

FIG. 2. Relationship between $\hat{\alpha}$ and precipitation P as inferred from the scaling in Eq. (53). In this plot, P is estimated as $P = \mathrm{W}_w S_p \mathrm{P}/(Lg)$. For this plot, $\mathrm{R} = 0.02$ J kg s^{-1} and $S_p = 2$ J kg^{-1} Pa^{-1}, a value that yields $\mathrm{c} = 50$ m s^{-1}.

By expanding Eq. (18b), combining it with Eqs. (49)–(51), and using the scales in Eq. (30) we find that W_w scales as

$$\mathrm{W}_w = \frac{\mathrm{R}}{\mathrm{S}_0(1-\hat{\alpha})}, \tag{52a}$$

where

$$\hat{\alpha} = \frac{\mathcal{L}_p}{\mathrm{S}_0} \tag{52b}$$

will be referred to as the Chikira (2014) scale, the ratio between the vertical gradients of latent energy and DSE. Close inspection of Eq. (52a) reveals that humid regions will exhibit much larger vertical velocities than dry regions for a fixed value of R. This is consistent with the idea that $1-\hat{\alpha}$ is proportional to the gross moist stability (Raymond et al. 2009; Sobel and Maloney 2013; Adames and Kim 2016; Adames and Maloney 2021). In humid regions, convection is less efficient at exporting MSE, requiring more convection to maintain thermodynamic balance in the region (Neelin and Held 1987; Raymond et al. 2009). The stronger convection when $\hat{\alpha}$ is near unity results in an exponential increase in precipitation, as seen in Fig. 2. In this scale analysis, $\hat{\alpha}$ works as a proxy for the column-integrated water vapor. Hence, the WTG scaling performed here is consistent with the observed relationship between column water vapor and precipitation (Bretherton et al. 2004; Rushley et al. 2018).

It is worth noting that the scaling for W_w breaks down when $\hat{\alpha} = 1$. This is due to the assumption that the vertical MSE advection by diabatic motions scales with Q_r, which becomes invalid when $\hat{\alpha} = 1$. A value of $\hat{\alpha}$ of unity is equivalent to a zero value of gross moist stability, which corresponds to zero net vertical import of MSE by convection (Benedict et al. 2014; Inoue and Back 2017; Adames et al. 2020). While this scenario is not discussed in this study, it is worth pointing out that an analysis of this case would require scaling W_w differently.

With the aforementioned definitions, we can obtain a nondimensional form of Eq. (18b), which we write as

$$\epsilon \frac{\mathrm{U}}{\mathrm{c}_p} \hat{\mathbf{v}}_w \cdot \hat{\boldsymbol{\nabla}}_h \hat{s} - \hat{\omega}_w \hat{S}_p = \hat{\alpha}\hat{Q}_c + (1-\hat{\alpha})\hat{Q}_r. \tag{53}$$

Examination of Eq. (53) reveals that in humid regions ($\hat{\alpha} \sim 1$ and $1-\hat{\alpha} \sim 0.1$), vertical velocities are governed by convective motions while in dry regions convective motions are negligible and the leading balance is between vertical DSE advection and radiative cooling.

We now use the results from this subsection to scale Eq. (4d). By combining Eqs. (37)–(52a) we obtain the following:

$$\mathrm{N}_w\left(\frac{\partial \hat{s}}{\partial \hat{t}} + \frac{\mathrm{U}}{\mathrm{c}_p}\hat{\mathbf{v}} \cdot \hat{\boldsymbol{\nabla}}\hat{s}\right) - \hat{\omega}\hat{S}_p = \hat{\alpha}\hat{Q}_c + (1-\hat{\alpha})\hat{Q}_r, \tag{54a}$$

where

$$\mathrm{N}_w = \max(\mathrm{Fr}_\tau^2, \mathrm{Bu}^{-1}). \tag{54b}$$

Note that the capital N in N_w is used to refer to a nondimensional number, and should not be confused with the Brunt–Väisälä frequency. The nondimensional vertical velocity scales as

$$\hat{\omega} = \hat{\alpha}\hat{\omega}_c + (1-\hat{\alpha})\hat{\omega}_r + \mathrm{N}_w\hat{\omega}'. \tag{54c}$$

Examination of Eq. (54) shows that vertical motions will always be in the leading-order balance. The WTG approximation is valid as long as $\mathrm{N}_w \ll 1$ and $\mathrm{N}_w \mathrm{U}/\mathrm{c}_p \leq 1$.

e. *Potential vorticity*

With the vorticity and thermodynamic equations scaled, it is instructive to consider the scaling for potential vorticity. First, we consider what component of PV governs its evolution. By expanding the local time derivative, we obtain the following:

$$\frac{\partial \mathrm{PV}}{\partial t} = gS_p\frac{\partial \zeta}{\partial t} + g\zeta_a\frac{\partial S_p}{\partial t}, \tag{55}$$

which we can make nondimensional by using Eqs. (39), (48), (45), and (47), yielding

$$\begin{aligned}\frac{\partial \hat{\mathrm{PV}}}{\partial \hat{t}} = {} & (1-\epsilon)\frac{\mathrm{L}_x}{\mathrm{L}_y}\mathrm{Ro}\left(\frac{\partial \hat{s}_0}{\partial \hat{p}} + \epsilon\frac{\mathrm{U}}{\mathrm{c}_p}\frac{\partial \hat{s}'}{\partial \hat{p}}\right)\frac{\partial \hat{\zeta}}{\partial t} \\ & + \epsilon\frac{\mathrm{U}}{\mathrm{c}_p}\left[(1-\epsilon)\frac{\mathrm{L}_x}{\mathrm{L}_y}\mathrm{Ro}\hat{\zeta} + \hat{f}\right]\frac{\partial^2 \hat{s}'}{\partial \hat{t}\partial \hat{p}}.\end{aligned} \tag{56}$$

Equation (56) reveals that when $\epsilon \ll 1$ the PV tendency is governed by the vorticity tendency. Furthermore, deviations of S_p from the global-mean value can also be neglected, making PV a scaled vorticity.

Following the previous subsections, we can make the PV budget nondimensional. By combining Eqs. (30), (39), and (46c), we obtain the following:

$$\frac{\mathrm{Ro}_\tau}{\mathrm{Ro}}\frac{\partial \hat{\mathrm{PV}}}{\partial \hat{t}} + \hat{\mathbf{v}}\cdot\hat{\boldsymbol{\nabla}}_h\hat{\mathrm{PV}} + \hat{\epsilon}\hat{\omega}\frac{\partial \hat{\mathrm{PV}}}{\partial \hat{p}} = \frac{\mathrm{U}_w}{\mathrm{U}}\left\{\mathrm{Ro}\,\frac{\mathrm{L}_y}{\mathrm{L}_x}\frac{\partial \hat{v}}{\partial \hat{p}}\frac{\partial \hat{Q}}{\partial \hat{x}} - \mathrm{Ro}\,\frac{\mathrm{L}_x}{\mathrm{L}_y}\frac{\partial \hat{u}}{\partial \hat{p}}\frac{\partial \hat{Q}}{\partial \hat{y}} - [\mathrm{Ro}(1-\epsilon)\hat{\zeta} + \hat{f}]\frac{\partial \hat{Q}}{\partial \hat{p}}\right\}, \tag{57}$$

which shows that none of the terms in the budget are negligible for scales that are characteristic of tropical motions.

f. Moisture budget

To obtain a relationship for q in terms of other variables, we will assume that the moisture tendency is on the same order of magnitude as the vertical MSE advection by convection. By using the scales in Eq. (30) along with Eqs. (50), (52a), and (53) we obtain the following:

$$L\mathrm{q} \sim \hat{\alpha}\tau\mathrm{R}, \tag{58}$$

revealing that for a fixed R, moisture anomalies are larger at longer time scales and more humid environments. We also assume that F_m is also of the same magnitude as the vertical MSE advection by convection, yielding the scaling $\mathrm{F} \sim \hat{\alpha}\mathrm{R}$.

By using Eq. (58) in combination with Eq. (30), we obtain the following nondimensional moisture budget:

$$\frac{\partial \hat{q}}{\partial \hat{t}} = -\frac{\mathrm{U}}{\mathrm{c}_p}\left(\hat{\mathbf{v}}\cdot\hat{\boldsymbol{\nabla}}_h\hat{q} + \frac{\epsilon}{1-\hat{\alpha}}\hat{\mathbf{v}}_c\cdot\hat{\boldsymbol{\nabla}}_h\hat{s}\right) - \hat{\omega}_c\frac{\partial \hat{m}}{\partial \hat{p}} - \left(\frac{\mathrm{N}_w}{1-\hat{\alpha}}\hat{\omega}' + \hat{\omega}_r\right)\frac{\partial \hat{q}}{\partial \hat{p}} - \frac{\partial \hat{F}_m}{\partial \hat{p}}, \tag{59}$$

which shows that vertical moisture advection by dry adiabatic lifting can play an nonnegligible role in the moisture budget of tropical systems, as Adames et al. (2021) pointed out. In a humid atmosphere ($1-\hat{\alpha} \ll 1$), adiabatic lifting by vertical moisture advection is on the same order of magnitude as the other terms when $\mathrm{N}_w \geq 0.1$.

g. Moist static energy

We can follow a similar procedure as was done with Eqs. (4d) and (4e) to obtain a nondimensional MSE equation:

$$\hat{\alpha}\frac{\partial \hat{m}}{\partial \hat{t}} = -\hat{\alpha}\frac{\mathrm{Ro}}{\mathrm{Ro}_\tau}\hat{\mathbf{v}}\cdot\hat{\boldsymbol{\nabla}}\hat{m} - \hat{\omega}\frac{\partial \hat{m}}{\partial \hat{p}} + \hat{Q}_r - \hat{\alpha}\frac{\partial \hat{F}_m}{\partial \hat{p}}, \tag{60}$$

where we define the nondimensional MSE as

$$\hat{m} \sim \mathrm{N}_{\mathrm{mode}}\hat{s} + \hat{q}, \tag{61}$$

where

$$\mathrm{N}_{\mathrm{mode}} \equiv \frac{\mathrm{N}_w}{\hat{\alpha}(1-\hat{\alpha})} \tag{62}$$

is a nondimensional scale that describes the relative contribution of moisture and DSE to the evolution of MSE. Adames et al. (2019) showed that when $\mathrm{N}_{\mathrm{mode}} \gg 1$, temperature governs the thermodynamics of the wave and the resulting behavior is that of gravity waves. When $\mathrm{N}_{\mathrm{mode}} \ll 1$, moisture governs the thermodynamics of a wave, resulting in moisture modes. A similar quantity to $\mathrm{N}_{\mathrm{mode}}$ was derived by Ahmed et al. (2021). A comparison of the definition of $\mathrm{N}_{\mathrm{mode}}$ from Adames et al. (2019) and the one in Eq. (62) is shown in SI section 4.

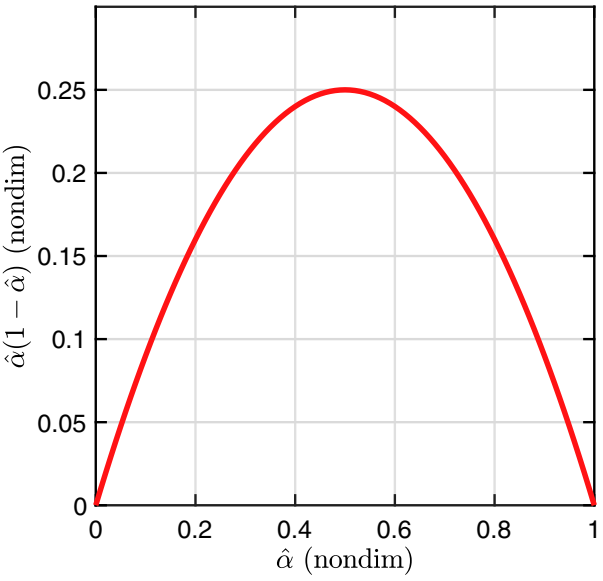

FIG. 3. Distribution of $\hat{\alpha}(1-\hat{\alpha})$ as a function of $\hat{\alpha}$.

The terms in Eq. (62) require some further explanation. From Eq. (58), we see that moisture increases linearly with $\hat{\alpha}$. From Eq. (52a) we see that convective vertical motions scale with the inverse of $1-\hat{\alpha}$. In the absence of gravity waves, the convection would heat the atmosphere at a rate that is inversely proportional to $1-\hat{\alpha}$. Because gravity waves transport the heat that is generated by convection, it follows that T would still scale as the inverse of $1-\hat{\alpha}$. This result can also be obtained if we divide Eq. (54) by $1-\hat{\alpha}$ and examining the case when $\mathrm{N}_w \sim 1$, a scaling that corresponds to gravity waves that are forced by convective heating.

The fact that $\mathrm{N}_{\mathrm{mode}}$ contains a factor of $\hat{\alpha}(1-\hat{\alpha})$ in the denominator has important implications for the governing thermodynamics of motion systems. As shown in Fig. 3, $\hat{\alpha}(1-\hat{\alpha})$ is small for values of $\hat{\alpha}$ between 0 and 1, obtaining a maximum value of 0.25 when $\hat{\alpha} = 0.5$. Thus, the magnitude of $\mathrm{N}_{\mathrm{mode}}$ is largely determined by N_w.

5. Types of convectively coupled motions

In addition to elucidating the governing thermodynamics, the value of $\mathrm{N}_{\mathrm{mode}}$ is also related to the momentum balance in $\mathbf{v}'$. By considering Eqs. (31), (47), and (62), we find that small values of $\mathrm{N}_{\mathrm{mode}}$ are associated with a $\mathbf{v}'$ that is quasi nondivergent, while large $\mathrm{N}_{\mathrm{mode}}$ is associated with an irrotational $\mathbf{v}'$, as shown by Fig. 4. However, because nondivergent flow can come in a variety of forms, it follows that even similar values of

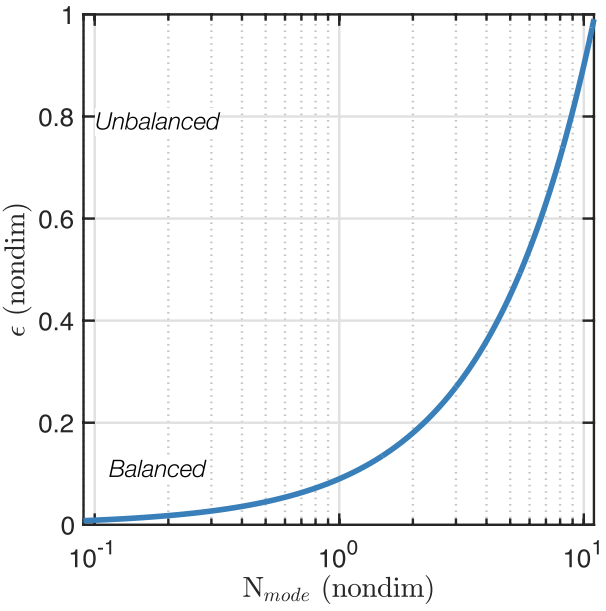

FIG. 4. Distribution of ϵ, which describes the fraction of $\mathbf{v}'$ that is irrotational, as a function of N_{mode} for the case when Bu ~ 100, which corresponds to $\lambda_y \sim (\pi/5)L_d$.

N_{mode} can be associated with different types of motion systems, even if the governing thermodynamics are similar. In this section, we will discuss seven types of convectively coupled motions that are found based on the scale analysis from the previous section. A summary of their scales is provided in Table 3 and a schematic that summarizes their features is shown in Fig. 5. From these scales we can obtain realistic values of the vertical velocity, zonal wind, temperature, and CWV for each type of motion with the only additional information needed being prescribing values for $\hat{\alpha}$, L_x, and R (Table 4).

a. *Convectively coupled inertio-gravity waves*

Convectively coupled inertio-gravity waves can exist when $N_{mode} \gg 1$ and $\hat{\alpha} \sim 1$, which arises when its propagation speed is close to the phase speed of dry gravity waves. To qualitatively understand why this is the case, we will use the shallow water dispersion relation of inertio-gravity waves [Eq. (11) in Matsuno 1966] and using an equivalent depth of $h = (1 - \hat{\alpha})g^{-1}c^2$, where the factor $\sqrt{1 - \hat{\alpha}}$ is used to account for convective coupling.[2] Plugging this dispersion on Eq. (62) yields the following scaling of N_{mode}:

$$N_{mode} \sim \frac{1}{\hat{\alpha}}\left[1 + \frac{(2n+1)}{(1-\hat{\alpha})^{1/2}}\frac{L_x^2}{L_e^2}\right], \tag{63}$$

where $L_e = \sqrt{c/\beta}$ is the equatorial radius of deformation, and the factor $2n + 1$ arises from Eq. (11) in Matsuno (1966).

Equation (63) shows that $N_{mode} \gg 1$ when the terms in square brackets are much greater than 1. Assuming that $\hat{\alpha} \sim 1$ and $1 - \hat{\alpha} \sim 0.1$ reveals that $L_x \geq 1.5\, L_e/(2n + 1)$ for N_{mode} to have a value of at least 10. It is worth noting that c = 50 m s^{-1} will yield inertio-gravity wave phase speeds that are too fast when compared to observations (Wheeler et al. 2000; Haertel and Kiladis 2004; Kiladis et al. 2009; Mayta and Adames 2021). This caveat can be ameliorated if we assume that they exhibit a second baroclinic vertical structure, in which case the characteristic phase speed of 25 m s^{-1} agrees better with observations. Thus, inertio-gravity waves are likely dominated by the second baroclinic vertical structure, as previous studies indicate (Mapes 2000; Haertel and Kiladis 2004). Assuming c = 25 m s^{-1} yields a zonal wavelength for $n = 0$ and $n = 1$ inertio-gravity waves of ~1×10^7 m and 4×10^6 m, respectively, which would correspond to zonal wavenumbers 4 and 10. These zonal scales are in agreement with the observed spectral peaks of the $n = 0$ and $n = 1$ inertio-gravity waves shown in Fig. 1 of Kiladis et al. (2009).

An alternative explanation is that inertio-gravity waves exhibit first baroclinic mode structure but are approximately in "convective quasi equilibrium" (Emanuel et al. 1994; Sobel and Bretherton 2003), i.e., instability is removed at a time scale that is much faster than the time scale of the wave (Ahmed et al. 2021). If this is the case, the value of N_{mode} will be closer to unity. Ahmed et al. (2021) showed that waves that are in quasi equilibrium exhibit anomalies in Lq and C_pT that are comparable in magnitude.

When examining the magnitudes for the different field variables that are consistent with inertio-gravity wave scaling (Table 4), we find that these waves exhibit zonal winds on the order of 3 m s^{-1}, CWV anomalies on the order of 0.1 mm and precipitation rates of 10 mm day^{-1}.

b. *Moisture modes*

Moisture modes occur when $N_{mode} \ll 1$, and thus require N_w to be on the order of 10^{-2} or less. Because of this constraint, moisture modes will always be slowly evolving, balanced systems with phase speeds of on the order of 5 m s^{-1} or less. They also require that Bu $\geq$ 100, implying that $\lambda_y \leq (\pi/5)L_d$. For $f = 3 \times 10^{-5}$ s^{-1} and c = 50 m s^{-1}, we obtain that $L_d = 1.6 \times 10^6$ m, and hence $\lambda_y \leq 10^6$ m. The adiabatic vertical motions are ~100 times weaker than their diabatic vertical motions, making their contribution to the evolution of moisture [Eq. (59)] negligible.

When examining Eqs. (34) and (62) we can identify two types of moisture modes.

1) EQUATORIAL MOISTURE MODES

One possibility that satisfies the $N_{mode} \ll 1$ requirement involves slowly propagating waves in which $Ro_\tau \ll 1$ and $L_y \ll L_x$. The resulting waves are characterized by a planetary scale in the zonal direction ($\lambda_x \sim 10^7$ m) and a meridional scale on the order of 10° ($\lambda_y \sim 10^6$ m). According to Eq. (34), these systems are in semigeostrophic balance, i.e., the meridional momentum

[2] Convectively coupled waves are usually analyzed using an equivalent depth which accounts for their slower propagation. In shallow water models, this slowdown is proportional to the square root of the normalized GMS ($\tilde{M}$) (Frierson 2007; Adames et al. 2019; Ahmed et al. 2021). In this study, $\hat{\alpha} \sim 1 - \tilde{M}$.

TABLE 3. Types of convectively coupled motions obtained from scale analysis, their related scaling parameters, and leading momentum balance. For all waves, a first baroclinic vertical structure is assumed (c = 50 m s^{-1}), except for inertio-gravity waves in which a second baroclinic structure is assumed (c = 25 m s^{-1}). For the scaling values obtained here a value of f of 3×10^{-5} s^{-1} is assumed.

Motion type	Ro_τ	Fr_τ^2	c_p (m s^{-1})	L_y/L_x	N_{mode}	λ_x (m)	λ_y (m)	Balance in $\mathbf{v}'$
Equatorial moisture mode	0.1	0.01	5	0.1	0.1	10^7	10^6	Semigeostrophic
Off-equatorial moisture mode	1	0.005	3.5	1	0.1	10^6	10^6	Nonlinear
Equatorial mixed wave	1	0.1	16	0.1	1	3×10^6	3×10^5	Semigeostrophic
Off-equatorial mixed wave	1	0.1	16	1	1	3×10^6	3×10^6	Nonlinear
Tropical depression	1	0.005	3.5	1	1	10^6	10^6	Nonlinear
n = 1 inertio-gravity waves	1	1	25	0.5	10	4×10^6	2×10^6	Unbalanced
Moist QG	0.1	0.001	1.6	1	1	3×10^6	3×10^6	Geostrophic

equation is in geostrophic balance but the zonal momentum equation is not. This scaling is reminiscent of equatorial long waves (Heckley and Gill 1984; Ogrosky and Stechmann 2015), which leads us to refer to these as "equatorial moisture modes." In these systems, temperature anomalies of 0.5 K are associated with zonal winds on the order of 10 m s^{-1}. The structure and propagation characteristics of this mode are reminiscent of the MJO's signature over the warm pool, which many studies have indicated has properties of a moisture mode (Raymond and Fuchs 2009; Sobel and Maloney 2013; Adames and Kim 2016; Jiang et al. 2018). Equatorial Rossby waves may also belong to this category of waves, as previous research has suggested (Gonzalez and Jiang 2019; Fuchs-Stone et al. 2019; Inoue et al. 2020; Mayta et al. 2022).

2) OFF-EQUATORIAL MOISTURE MODES

Another possibility that also yields moisture modes involves a value of $Ro_\tau \sim 1$ and $L_y \sim L_x$. These systems would exhibit a horizontal wavelength of 1000 km or less and a wind field that is in nonlinear balance. This description is reminiscent of off-equatorial vortices such as tropical depressions, and hence will be referred to as off-equatorial moisture modes. Eastern Pacific easterly and monsoon low pressure systems waves may also fit in this category, as they exhibit large moisture anomalies and tend to propagate slowly (Serra et al. 2008; Rydbeck and Maloney 2015; Wolding et al. 2020; Clark et al. 2020; Diaz and Boos 2021).

In these systems, zonal winds on the order of 3 m s^{-1} are associated with temperature anomalies of 0.1 K and precipitation rates on the order of 30 mm day^{-1} (Table 4) when $\hat{\alpha} \sim 0.95$. The scaling of these systems suggest that they become stronger as $\hat{\alpha} \to 1$ and will propagate slower.

c. *Mixed systems*

As mentioned previously, when $N_{mode} \sim 1$, temperature and moisture play roughly equal roles in the thermodynamics of tropical motion systems. Because the resulting behavior is

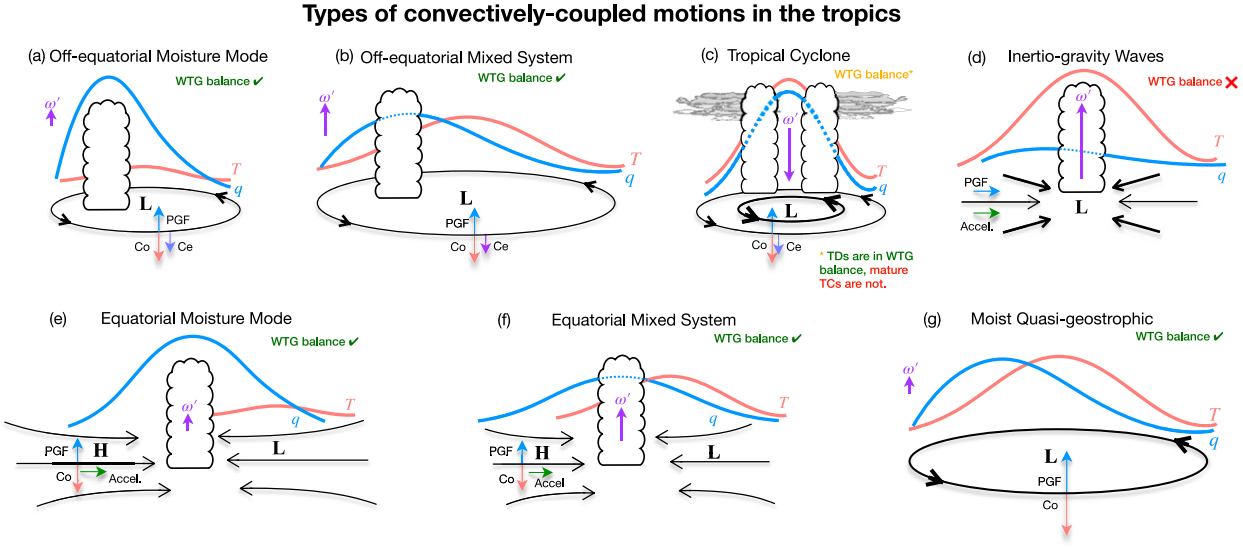

FIG. 5. Schematic showing the horizontal structure and relative amplitude of T and q in the seven types of convectively coupled motions described in Table 3: (a) off-equatorial moisture modes, (b) off-equatorial mixed system, (c) TCs, (d) inertio-gravity waves, (e) equatorial moisture modes, (f) equatorial mixed system, and (g) moist QG motions. The horizontal circulation is shown in black, with the governing momentum balances shown in arrows (PGF = pressure gradient force, Co = Coriolis force, Ce = centrifugal force). The qualitative amplitude of moisture is shown in blue while the amplitude of temperature is shown in salmon. The amplitude of ω' is shown as a light purple arrow. Systems that are in WTG balance are denoted with green text while those that are not in WTG balance are denoted in red.

TABLE 4. Realistic scaling values obtained for the six categories of coupled dynamic–thermodynamic regimes that can exist in a moist atmosphere. Each value is obtained from the scales in Table 3 and assuming R = 0.02 J kg s^{-1}, S_0 = 2 J kg^{-1} Pa^{-1}, and $f = 3 \times 10^{-5}$ s^{-1}, along with the values of $\hat{\alpha}$ provided. The CWV anomalies (CWV′) are obtained as CWV = $C_p qP/(Lg)$.

Motion type	$\hat{\alpha}$	W_w (Pa s^{-1})	W′ (Pa s^{-1})	U (m s^{-1})	T (K)	CWV (mm)	P (mm day^{-1})
Equatorial moisture mode	0.9	0.1	10^{-3}	10	0.5	5	10
Off-equatorial moisture mode	0.95	0.3	10^{-3}	3	0.1	0.5	30
Equatorial mixed wave	0.9	0.1	10^{-2}	3	0.5	0.5	10
Off-equatorial mixed wave	0.9	0.1	10^{-2}	3	0.5	0.5	10
Tropical depression	0.95	0.3	0.1	15	1	0.5	30
$n = 1$ inertio-gravity waves	0.9	0.1	0.1	3	1	0.1	10
Near-stationary moist QG	0.5	10^{-2}	10^{-3}	10	1	1	1

rather ambiguous, possibly having elements of moisture modes, gravity waves, or even QG systems, we will refer to these systems as mixed. As in the case of moisture modes, the scale analysis presented in the previous section allows for two possible types of mixed systems.

1) EQUATORIAL MIXED SYSTEM

One possibility that yields $N_{mode} \sim 1$ is when $Fr_\tau^2 \sim 10^{-1}$ and when $L_y^2 \ll L_x^2$ and $Ro_\tau \sim 1$. In such a case the system would exhibit a phase speed of ~16 m s^{-1}, and a horizontal wavelength of 3000 km. In accordance with Eq. (34), these systems are in semigeostrophic balance, as in equatorial moisture modes, but are shorter in wavelength and propagate ~3 times faster. As shown in Table 4, these systems are characterized by zonal winds of 3 m s^{-1}, temperature anomalies of ~0.5 K, CWV anomalies of 0.5 mm, and precipitation rates of 10 mm day^{-1}. The scales that represent this type of system are reminiscent of a convectively coupled Kelvin wave (Wheeler et al. 2000; Straub and Kiladis 2003; Kiladis et al. 2009; Mayta et al. 2021). If we use the equivalent shallow water dispersion of Kelvin waves (Kiladis et al. 2009; Frierson 2007; Ahmed et al. 2021), we find that in these systems $N_{mode} \sim \hat{\alpha}^{-1}$, indicating that Kelvin waves are mixed systems in a humid atmosphere where $\hat{\alpha} \sim 1$.

2) OFF-EQUATORIAL MIXED SYSTEM

The other variant of a mixed system occurs when both L_y/L_x and Ro_τ are near unity. In this case, the system is in nonlinear balance according to Eq. (34) and Fig. 4. The scaling values for this system largely mirror that of the equatorial mixed system, except the zonal and meridional wavelength are of similar value at ~1000–3000 km. Given these values, off-equatorial mixed systems are most reminiscent of African easterly waves (Burpee 1974; Kiladis et al. 2006; Diaz and Aiyyer 2013).

d. Tropical cyclones

A special case of the scaling presented here occurs when $Ro \gg Ro_\tau$, i.e., $U \gg c_p$. Under this scaling $U' \gg U_w$ and the relative vorticity that is much larger than f. As a result, the deformation in these systems is $L_d = c/\zeta$ (Ooyama 1982), and the WTG balance criterion becomes $N_w = Fr^2 = U^2/c^2$. Two scenarios can be obtained from this scaling. The first one corresponds to tropical depressions, which are characterized by temperature anomalies on the order of 1 K, and horizontal winds of ~15 m s^{-1}, and $N_w \sim 0.1$ (Table 4). Thus, even though horizontal DSE advection can be large compared to the other tropical motions described here, they are still an order of magnitude smaller than the vertical DSE advection. Thus, tropical depressions are approximately in WTG balance according to the scaling presented here. Since $N_w \sim 0.1$ it follows that N_{mode} exhibits a value of unity or larger. Hence, tropical depressions are not moisture modes. In spite of this categorical difference, off-equatorial moisture modes are identical to tropical depressions except that their horizontal winds are weaker. Given their similarities, it is possible that off-equatorial moisture modes are tropical depression precursors. The other scaling corresponds to U ~ c, which corresponds to a mature TC. Under this scaling $N_w \sim 1$. Hence, mature TCs are not in WTG balance.

e. Moist QG motions

The scaling presented in the previous section allows for moist QG dynamics in the tropics. This occurs when (Ro_τ, Ro) $\ll 1$ and Bu ~1. Following these constraints, we find that realistic scales for L_x, U, and T are possible when $Fr^2 \sim 10^{-3}$ and $\hat{\alpha} \leq 0.5$. Otherwise, the wind speed and vertical velocity scales become unrealistically large. In such a case we find that $N_{mode} \sim 1$, $L_x \sim 3000$ km, U ~ 10 m s^{-1}, and T ~ 1 K. That N_{mode} is near unity indicates that moisture and temperature play comparable roles in the thermodynamics of moist QG motions. Interestingly, these systems are in WTG balance since $N_w \sim 0.1$. Because of the smallness of Fr_τ^2, moist QG motions are restricted to near stationary systems. Furthermore, because realistic values for the scales are only possible if $\hat{\alpha} \leq 0.5$, it follows that these systems are more likely to occur in the subtropics. A possible example of a moist QG system may be the tropical upper-tropospheric trough (Sadler 1976; Ferreira and Schubert 1999), or the equatorial stationary waves (Grise and Thompson 2012).

f. Comparison

Of the seven types of convectively coupled systems summarized in Tables 3 and 4, we find that equatorial moisture modes exhibit the largest zonal scales. After TCs, they exhibit the largest wind speeds at 10 m s^{-1}. Based on this scaling we would expect equatorial moisture modes to be among the most prominent systems in the tropics. This is consistent with the strong MJO signal seen in spectral analysis of OLR and u done by multiple studies (Wheeler and Kiladis 1999; Roundy

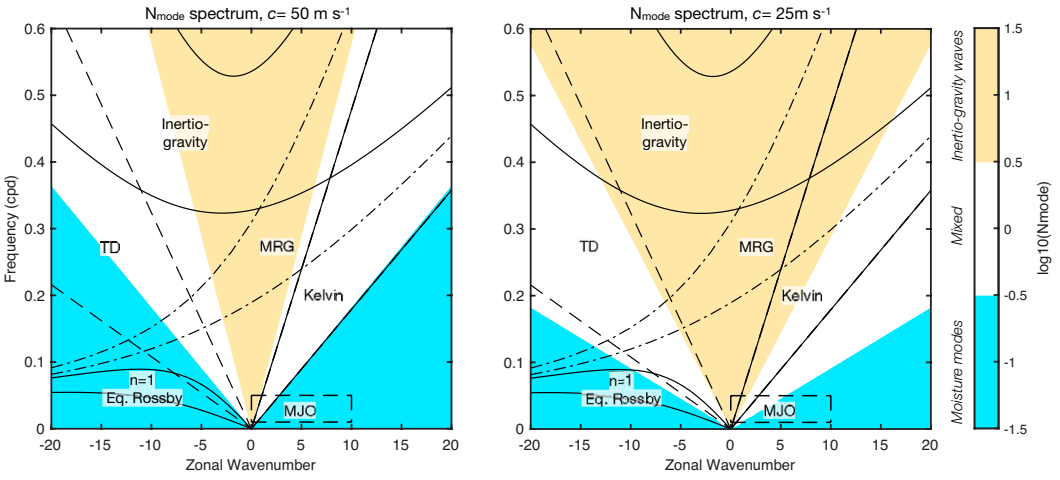

FIG. 6. Wavenumber–frequency distribution of base 10 logarithm of N_{mode} for an atmosphere where $\alpha \sim 0.9$ for motion systems in which Bu $\sim$ 100. Blue shading represents systems that can be considered moisture modes, the yellow shading represents inertio-gravity waves and white represents mixed systems. The solid lines corresponds to the dispersion curves of $n = 1$ inertio-gravity waves, Kelvin waves and $n = 1$ equatorial Rossby waves, while the dot–dash line corresponds to the dispersion curve of mixed Rossby–gravity waves. The lines are shown for equivalent depths of 8 and 50 m. The dashed box shows the wavenumber–frequency band where the MJO's spectral signature is observed while the dashed lines show constant phase speeds of 5 and 15 m s^{-1}, which enclose tropical depression-like (TD) disturbances and easterly waves (Kiladis et al. 2006; Yasunaga and Mapes 2012; Adames and Ming 2018).

and Frank 2004; Hendon and Wheeler 2008). The other six types of motion systems identified can be considered synoptic-scale or mesoscale systems since their horizontal scale is on the order of 1000 km or less.

When comparing the off-equatorial moisture mode, the two mixed systems and inertio-gravity waves, we find that they exhibit comparable magnitudes in their horizontal scale, winds, and precipitation rates. Their main difference lies in their propagation speed, as would be expected from N_{mode}, which is also associated with the governing forces in the momentum equation, as shown in Table 3.

In spite of these dynamic and thermodynamic differences, six of the seven types of motions exhibit precipitation rates on the order of 10 mm day^{-1} or larger, perhaps an indicator that they may couple to convection through different processes. Only moist QG systems have realistic scales that result in lower precipitation rates.

While Table 3 shows typical parameters for these motion systems, it is important to point out that these can exist over a wide variety of scales. To gain some additional perspective, the space–time spectral distribution of N_{mode} can be plotted and compared with the typical dispersion curves of observed convectively coupled equatorial waves, as in Adames et al. (2019). In Fig. 6 we see this distribution for c = 50 and 25 m s^{-1}, which correspond to first and second baroclinic vertical structure. While changing the value of c does change the distribution of N_{mode} somewhat, the main features remain the same. From examination of Fig. 6 we see that equatorial Rossby waves fall well within the moisture mode part of the spectrum. Most of the MJO band does as well, except for the zonal wavenumber 1 part of the signal. Previous work has indicated that this component of the MJO may not be a moisture mode (Powell 2017; Fuchs and Raymond 2017; Adames et al. 2019; Emanuel 2020; Ahmed et al. 2021; Snide et al. 2022), and it is well established that the circumnavigating component of the MJO signal outside of the warm pool exhibits features that are more akin to a Kelvin wave (Sobel and Kim 2012).

Mixed Rossby–gravity and inertio-gravity waves are in the inertio-gravity part of the spectrum. Kelvin waves and TD-like disturbances lie in the mixed region, although slow, first baroclinic TD waves are well within the moisture mode regime, while fast, second baroclinic Kelvin waves are well in the inertio-gravity wave regime.

6. Simplified basic equations under WTG balance

a. *Approximations for slow tropical motions*

We will now use the results of the scale analysis to simplify the basic equations under the conditions in which the WTG approximation is applicable, which requires that $\text{N}_w \gg 1$. Under this scaling, we can drop all the small terms from the thermodynamic equation [see Eqs. (20d), (48), and (54)] to obtain the following:

$$S_{p_0} \nabla_h^2 X_w \simeq Q, \tag{64}$$

where $S_{p_0} = -\partial_p s_0$ is the global mean value of the static stability. When $\text{N}_w \ll 1$, $\epsilon \ll 1$ (Fig. 4) and thus $\mathbf{v}'$ is approximately nondivergent [Eq. (31)]:

$$\nabla_h \cdot \mathbf{v}' \simeq 0. \tag{65}$$

Thus, the total horizontal wind is composed of a irrotational component that is in exact WTG balance and a quasi-nondivergent deviation from this strict balance:

$$\mathbf{v} \simeq \frac{\partial}{\partial p}(\boldsymbol{\nabla}_h X_w) + \mathbf{k} \times \boldsymbol{\nabla}_h \psi'. \tag{66}$$

The quasi nondivergence of $\mathbf{v}'$ implies that the winds are parallel to the height surfaces, and hence ψ' and Φ are directly related. Based on this scaling result, it reasonable to assume that $\mathbf{v}'$ is in nonlinear balance. Hence Φ can be written in terms of ψ' as follows:

$$\nabla_h^2 \Phi' \simeq \boldsymbol{\nabla}_h \cdot (f \boldsymbol{\nabla}_h \psi') + 2\mathbf{k} \cdot \left(\frac{\partial \boldsymbol{\nabla}_h \psi'}{\partial x} \times \frac{\partial \boldsymbol{\nabla}_h \psi'}{\partial y} \right). \tag{67}$$

With this definition, Σ can be written in terms of X_w and ψ':

$$\Sigma \simeq \beta \frac{\partial^2 X_w}{\partial x \partial p} - 2\left[\mathbf{k} \cdot \left(\frac{\partial \boldsymbol{\nabla}_h X_w}{\partial p \partial x} \times \frac{\partial \boldsymbol{\nabla}_h X_w}{\partial p \partial y} \right) + \det(\mathbf{A}) \right], \tag{68}$$

where the terms on the rhs are the horizontal divergence of the Coriolis acceleration of $\mathbf{v}_w$, a solenoidal term involving the gradient of the WTG winds, and

$$\mathbf{A} = \begin{bmatrix} \dfrac{\partial^2 \psi'}{\partial x \partial y} & \left(\dfrac{\partial^2}{\partial x^2} - \dfrac{\partial^2}{\partial y^2} \right) \psi' \\ \dfrac{\partial^2 \chi_w}{\partial x \partial y} & \left(\dfrac{\partial^2}{\partial x^2} - \dfrac{\partial^2}{\partial y^2} \right) \chi_w \end{bmatrix} \tag{69}$$

can be thought of as a tensor that describes the spatial displacement and anisotropy between χ_w and ψ'. It is written in terms of χ_w rather than X_w to make the symmetry of the terms clear, and the nomenclature is chosen to allude to the anisotropy tensor discussed in Hoskins et al. (1983).

From examination of the terms on the rhs in Eq. (68) we see that the first two terms are only functions of X_w. Only the tensor $\mathbf{A}$ has contributions from ψ', implying that it contributes to Σ when there is an anisotropy and/or a spatial displacement between χ_w and ψ'. It is worth pointing out that Eq. (68) is the residual of the difference of the terms in Eq. (7), and its accuracy depends on the accuracy of the approximation in Eq. (67). Since Eq. (67) becomes more exact as ϵ (and hence N_w) become smaller, it follows that Eq. (68) is most accurate for moisture modes since they are the slowest motion systems discussed in section 5. Nonetheless, the potential residual that may exist in Eq. (68) from deviations from WTG balance is a caveat of this study.

Under conditions in which the WTG approximation is valid, the PV budget can be simplified by dropping all the small terms in Eqs. (56) and (57). Thus, the evolution of PV is approximately described by the evolution of the absolute vorticity:

$$\frac{\partial \mathrm{PV}}{\partial t} \simeq g S_{p_0} \frac{\partial \zeta_a}{\partial t}. \tag{70}$$

From Eq. (65) it follows that $\delta \simeq \delta_w$. Hence, Eq. (6) becomes an equation that describes the evolution of the component of the circulation that is in strict WTG balance.

b. *The "WTG equations" for slow tropical motions*

The aforementioned simplifications, which are based on the constraint that the motion system evolves slowly enough that the irrotational flow is in WTG balance and the nondivergent deviation from WTG balance is in nonlinear balance allows us to turn Eqs. (16) and (6) into what we will refer to as the "WTG equations":

$$\frac{\partial \zeta}{\partial t} = -\boldsymbol{\nabla}_h \cdot \left(\mathbf{v} \zeta_a - \omega_w \mathbf{k} \times \frac{\partial \mathbf{v}}{\partial p} \right), \tag{71a}$$

$$\frac{\partial \delta_w}{\partial t} = -\boldsymbol{\nabla}_h \cdot \left(\mathbf{v} \delta_w + \omega_w \frac{\partial \mathbf{v}}{\partial p} \right) - \Sigma. \tag{71b}$$

Through the use of Eqs. (14b), (20), (24), (66), and (68) we see that all variables in Eqs. (71a) and (71b) can be expressed in terms of ψ' and X_w. Thus, Eqs. (71a) and (71b) form a closed system of equations. It is worth noting that the first two terms on the rhs of (71a) and (71b) mirror one another. The first term is a horizontal flux while the second term involves ω_w and vertical changes in $\mathbf{v}$. Only the term Σ has no analog in the vorticity equation. It is also worth pointing out that Eq. (71a) is identical to the WTG vorticity equation shown in Raymond et al. (2015), except we are showing it in isobaric coordinates and excluding the frictional term. For completeness, we show the WTG equations with friction in SI section 6.

The terms on the rhs of Eq. (71a) represent the sum of vorticity advection, vortex stretching and vortex tilting. They can also be understood as the horizontal divergence of $\mathbf{J}(gS_{p_0})^{-1}$. However, the terms on the rhs of Eq. (71b) warrant further discussion. To better understand these terms, Fig. 7a shows an idealized vortex and a region of convergence that is shifted to its southwest. Details on the construction of Fig. 7 is shown in SI section 5. Subsequent panels show the terms on the rhs of Eq. (71b), except for $-\boldsymbol{\nabla}_h \cdot (\omega_w \partial_p \mathbf{v})$ as we are assuming the map corresponds to a region in the lower free troposphere where this term is small. The term $-\boldsymbol{\nabla}_h \cdot \mathbf{v}\delta_w$ (Fig. 7a) acts to advect the region of convergence downstream as well as concentrate it. Figures 7c–e show the individual contributions of the terms in Σ to the divergence tendency. The term $-\beta u_w$ is much weaker than $-\boldsymbol{\nabla}_h \cdot \mathbf{v}\delta_w$, and acts to shift the region of convergence westward. The solenoidal term of the WTG winds acts to weaken the region of convergence. The anisotropy term $\det(\mathbf{A})$ causes a convergence tendency to the north and northeast of the region of convergence, and a divergence tendency to the southeast (Fig. 7e). This term affects a larger area than the other terms, and tends to act in the opposite direction as $-\boldsymbol{\nabla}_h \cdot \mathbf{v}\delta_w$. It vanishes when the convergence is collocated with the vorticity and they have the same horizontal structure, as expected from an anisotropy tensor (SI Fig. 1).

The sum of the terms, shown in Fig. 7f, shows a pattern that is reminiscent of a pair of clockwise spirals. The magnitude of this tendency is on the order of 10^{-11} s^{-2}. Since the convergence in Fig. 7 is on the order of 10^{-6} s^{-1}, a value that is commonly seen in synoptic-scale motions (McBride and Gray 1980; Kiladis et al. 2006), it follows that the tendency in δ_w has

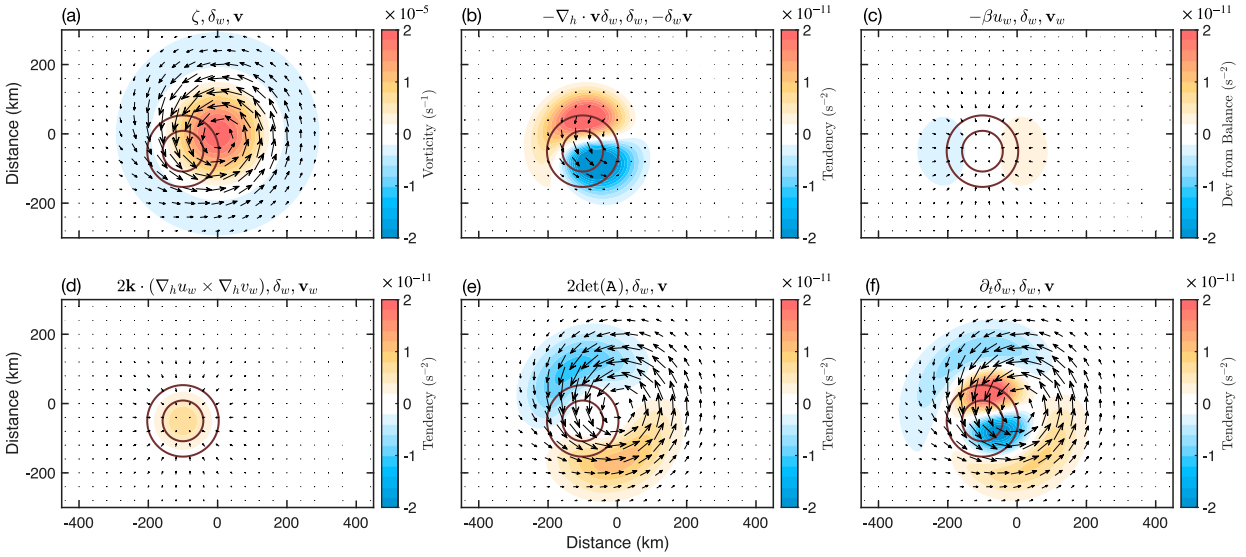

FIG. 7. (a) Horizontal map showing an idealized region of vorticity ζ (shading) and WTG convergence δ_w (contours). (b)–(f) The processes the lead to the evolution of δ_w: (b) convergence of the flux of divergence, (c) $-\beta u_w$, (d) the solenoidal term of the WTG winds, (e) the determinant of the tensor $\mathbf{A}$, and (f) the sum of the shaded terms in (b)–(e). The x and y axis denotes the distance from the center of vortex. The largest arrows correspond to winds of ~1 m s^{-1}. The processes shown in each in each panel are shown in the title in the following order: shading, contours, and arrows. The contour interval is 1.5×10^{-6} s^{-1}.

a time scale that is roughly on the order of a day ($\tau \sim 10^5$ s). If δ_w is associated with a vertical velocity that extends through the depth of the troposphere, then ω_w would exhibit a scale of ~10^{-1} Pa s^{-1} and the divergence tendency would be associated with a temperature tendency on the order of 10 K day^{-1} if the resulting motions were purely adiabatic. However, the resulting vertical motions are instead balanced by diabatic heating in order to maintain WTG balance. Thus, the processes that lead to the evolution of δ_w explain how Q evolves at the time scale of large-scale motion systems. Interestingly, because the terms in Figs. 7b and 7d are nonlinear, the resulting sum of terms is not a mirror opposite of Fig. 7f when we consider a region of WTG divergence (not shown).

The term $-\nabla_h \cdot (\omega_w \partial_p \mathbf{v})$ was not shown in Fig. 7 because it depends on the vertical structure of the vertical shear. Because of this, we instead this process schematically in Fig. 8. Since $-\nabla_h \cdot (\omega_w \partial_p \mathbf{v}) = -\partial_p \mathbf{v} \cdot \nabla_h \omega_w - \omega_w \partial_p \delta$, we can consider the two contributions separately and then add them. The term $-\partial_p \mathbf{v} \cdot \nabla_h \omega_w$, shown in Fig. 8a, induces a convergence tendency and hence upward acceleration downshear of the heating. This is the same process that causes thunderstorms to propagate downshear through a dynamically induced upward pressure gradient force (see chapter 8 in Houze 2014). The second term is the vertical advection of divergence (Fig. 8b), which increases convergence in the region where ω_w attains a maximum magnitude. Together,

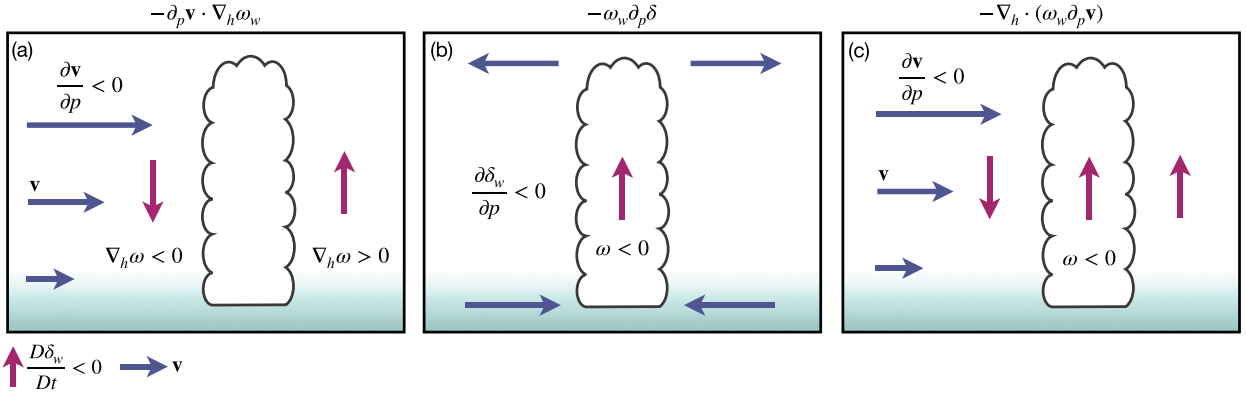

FIG. 8. Schematic describing how the term $-\nabla_h \cdot (\omega_w \partial_p \mathbf{v}) = -\partial_p \mathbf{v} \cdot \nabla_h \omega_w - \omega_w \partial_p \delta$ can induce a divergence tendency. (a) The contribution from $-\partial_p \mathbf{v} \cdot \nabla_h \omega_w$, (b) the contribution from $-\omega_w \partial_p \delta$, and (c) the sum. The cloud indicates a region of diabatic heating with the purple arrows depicting the horizontal flow, maroon arrows indicate direction of the vertical motion associated with the divergence tendency. The contours in the upper part of (a) and (c) denote the velocity potential.

the two terms cause increased convergence near and downshear of the region of maximum ascent.

c. Lagrangian form of the WTG equations

Additional insight on how a system that is in WTG balance evolves can be obtained by writing them in Lagrangian form. For (71a) this can be done by using the definition of the material derivative in Eq. (4g) and some rearrangement. For Eq. (71b), we use make use of the following identity:

$$\frac{\partial}{\partial p}\left(\frac{D\omega_w}{Dt}\right) = -\frac{D\delta_w}{Dt} + \frac{\partial \mathbf{u}}{\partial p}\cdot\boldsymbol{\nabla}\omega_w, \tag{72}$$

which we then combine with Eq. (6), and perform an integral with respect to pressure from $p = 0$. We will also define the integrated deviation from balance as

$$\{\Sigma\}(x,y,p,t) = \int_0^p \sum(x,y,p',t)dp'. \tag{73}$$

One can alternatively integrate from the pressure level p to a higher pressure where ω_w vanishes and get similar results. Following this procedure, we obtain the Lagrangian form of the WTG equations:

$$\frac{D\zeta_a}{Dt} = \boldsymbol{\eta}_a\cdot\boldsymbol{\nabla}\omega_w, \tag{74a}$$

$$\frac{D\omega_w}{Dt} = \{\Sigma\} + 2\left\{\frac{\partial \mathbf{u}}{\partial p}\cdot\boldsymbol{\nabla}\omega_w\right\}, \tag{74b}$$

where the material derivative is approximated as

$$\frac{D}{Dt} \simeq \frac{\partial}{\partial t} + \mathbf{v}\cdot\boldsymbol{\nabla}_h + \omega_w\frac{\partial}{\partial p}, \tag{74c}$$

where the term on the rhs of Eq. (74a) is the PV generation by the diabatic vertical velocity, the sum of vortex stretching and tilting. Diabatic vertical acceleration is in turn driven by the integrated deviation from nonlinear balance, as well as by integrated advection of ω_w by the total shear, including the vertical component.

The advantage of the Lagrangian form of the WTG equations shown in (74) is that it succinctly summarizes the evolution of a system that is in WTG balance. The Lagrangian tendency in absolute vorticity is nonzero only when ω_w is nonzero. Whether a resting parcel can accelerate upward is determined by the magnitude of the deviation from nonlinear balance Σ and by the dynamic pressure gradient force that is induced when there is ascent in the presence of shear. Parcels that are accelerating upward may also have accelerating rates of change in ζ_a since both $\boldsymbol{\eta}_a$ and $\boldsymbol{\nabla}\omega_w$ may be increasing with time.

d. Interpretation of the WTG equations

As mentioned in section 1, WTG balance is the result of the redistribution of temperature by gravity waves. This balance is quickly attained as these waves propagate away from the region of heating that forced them (see Fig. 2 in Adames and Maloney 2021). However, the predominantly irrotational non-WTG circulation in the propagating gravity waves quickly becomes deflected by the Coriolis and centrifugal forces, causing the non-WTG circulation to become nondivergent. As a result, the wave response to diabatic heating adjusts the system toward both WTG and nonlinear balance in X_w and ψ' in a manner that is analogous to geostrophic adjustment (see section 3.9 in Vallis 2017). In the WTG equations, this adjustment process is assumed to be instantaneous compared to the time scale of the motion system that they describe, hence why the deviation from WTG balance has no irrotational component.

To understand why the divergence equation describes the evolution of Q it will be convenient to write the terms on the rhs of Eq. (71b) as the divergence of a horizontal forcing vector $\mathbf{F}$:

$$\frac{\partial \delta_w}{\partial t} = \boldsymbol{\nabla}_h\cdot\mathbf{F}, \tag{75}$$

where

$$\mathbf{F} = -(\mathbf{u}\cdot\boldsymbol{\nabla})\mathbf{v} - f\mathbf{k}\times\mathbf{v} - \boldsymbol{\nabla}_h\Phi' \tag{76}$$

is the sum of momentum advection and the Coriolis and pressure gradient forces. We can interpret $\mathbf{F}$ as a flux of divergence by a forcing velocity $\mathbf{v}_F$, i.e., $\mathbf{F} = \delta_w\mathbf{v}_F$, so that

$$\frac{\partial \delta_w}{\partial t} = -\boldsymbol{\nabla}_h\cdot(\delta_w\mathbf{v}_F). \tag{77}$$

From Eq. (77) we see that Q is not being created or destroyed since the rhs vanishes when averaging globally. Rather, it is being redistributed by a nominal velocity $\mathbf{v}_F$ that results from the advection and forces that induce a local acceleration of the wind. Because $\mathbf{v}_F$ is horizontal Eq. (77) implies that, under WTG balance, δ_w obeys an impermeability principle to isobaric surfaces. Thus, the total flow becomes severely constrained. It must evolve in a way that maintains the nondivergent component in nonlinear balance and the irrotational component in WTG balance while also obeying impermeability principles in both the vorticity and divergence equations (Fig. 9).

7. Concluding discussion

In this study, we extended the weak temperature gradient (WTG) approximation (Sobel and Bretherton 2000; Sobel et al. 2001) to the full set of basic equations in isobaric coordinates on a rotating plane. Following previous studies (Mapes and Houze 1995; Adames et al. 2021), the vertical velocity is decomposed into a component that is in strict WTG balance, and a non-WTG residual. This decomposition is extended to the horizontal winds. While the strictly WTG-balanced winds are irrotational by construction, the deviation from strict WTG balance can have both an irrotational and nondivergent component.

Scale analysis was performed on the decomposed basic equations. The analysis differed from that of previous studies (Sobel et al. 2001; Yano and Bonazzola 2009; Adames et al.

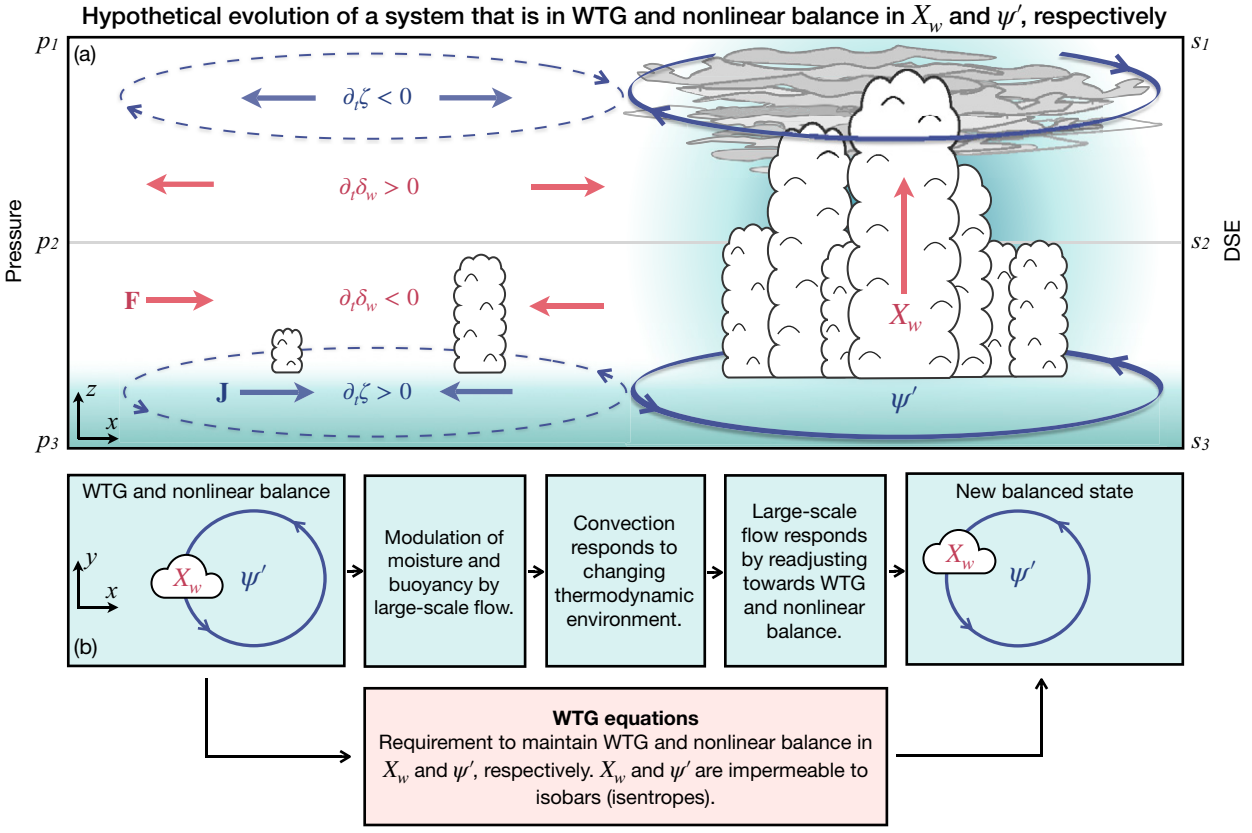

FIG. 9. Schematic describing how the WTG equations [Eqs. (71a) and (71b)] lead to the evolution of a slowly evolving tropical system. (a) The motion system is denoted by a lower- and upper-tropospheric circulation (indigo arrows) and the large-scale vertical velocity is denoted in red. The vorticity and divergence tendency are centered where the divergence of the horizontal forcing vectors **J** and **F** are a maximum, respectively (shown as a dashed contour). (b) A slowly evolving system hypothetically evolves both in accordance to changes in the thermodynamic environment and with the constraints of the WTG equations.

2019) in that it was applied to the observed tropical troposphere with the a priori decomposition of the wind field into strict WTG and deviation components. We found that the magnitude of the component of the horizontal flow that is in strict WTG balance is comparable to the deviation from this balance for most types of motion systems, as discussed by Sobel et al. (2001). Thus, most of the motions discussed here do not exhibit the so-called asymptotic nondivergence discussed by previous studies (Delayen and Yano 2008; Yano and Bonazzola 2009), QG motions and TCs being the exceptions. As a consequence of this scaling, it is more useful to consider the structure of the non-WTG component of the horizontal flow to determine whether a large-scale system is balanced or unbalanced in the momentum equations [Eqs. (31) and (47)]. It is found that slowly propagating systems the deviation from strict WTG balance is approximately nondivergent, while it is irrotational in fast systems, as posited by Raymond et al. (2015).

We also extended the results of Adames et al. (2019) by deriving a definition of N_{mode}—a nondimensional number that describes the magnitude of DSE tendency relative to the latent energy tendency—that is applicable to the full atmosphere. Unlike the N_{mode} derived by Adames et al. (2019), this definition does not make use of any convective parameterizations. While the scaling of moisture increases in proportion to the background moist stability ($\hat{\alpha}$), temperature in convecting regions scales as inversely proportional to $1 - \hat{\alpha}$. As a result, the relative magnitude of temperature with respect to moisture is not related so much by the moist stability, but by the structure and propagation characteristics of the systems as well as the dominant balances in the momentum equations.

Considering the thermodynamic scaling together with the scaling of the momentum equations reveals that convectively coupled tropical motions can come in at least seven forms that are summarized in Fig. 5 and in Tables 3 and 4. The seven identified systems are the equatorial and the off-equatorial moisture mode, equatorial and off-equatorial mixed systems, convectively coupled inertio-gravity waves, TCs, and moist QG systems. Their characteristics were discussed in section 5. Of the seven systems, only inertio-gravity waves and strong TCs are not in WTG balance.

The results of the scale analysis were also used to obtain a system of equations that describes the evolution of systems that are in WTG balance at the leading order. In these systems, the PV budget becomes an equation for the vertical

component of the absolute vorticity, as in Raymond et al. (2015). The component of the circulation that is in strict WTG balance can only increase vorticity locally through an effective flux that resembles a Coriolis force which contains the effects of diabatically driven vortex stretching and tilting (Fig. 1). The winds that deviate from strict WTG balance, in turn, drive a vorticity tendency predominantly through horizontal advection. The WTG-balanced circulation is described by the divergence equation, which can be turned into a vertical momentum equation. Sobel et al. (2001) also derived a WTG divergence equation in their Eq. (12). However, in their study the diabatic heating is prescribed, so they used it as a diagnostic equation for the height anomalies.

When irrotational and nondivergent components of the flow are in WTG and nonlinear balance, respectively, the vorticity and WTG divergence equations form a closed system of equations. That the WTG equations are closed implies we do not need to invoke neither the temperature nor moisture tendencies to understand the evolution of systems that are in WTG balance. This is an unexpected result, given the growing literature showing the importance of moisture in understanding tropical motions and its essential role in the existence of moisture modes. We hypothesize that the information on moisture is implicit in the definition of the integrated velocity potential X_w (Fig. 9b). One can envision the processes shown in Fig. 8 in terms of horizontal and vertical moisture advection, which in turn causes the diabatic heating to change with time. More work is needed to understand this finding.

There are several caveats to this study. First, while the scale analysis may provide a useful starting point to understand the nature of atmospheric motions, it may not always properly characterize them. For example, the scaling implies that as the troposphere nears saturation ($\hat{\alpha} \to 1$) N_{mode} would become infinite and hence moisture modes would not occur. However, simple models of equatorial waves with prognostic moisture show that the opposite occurs: moisture modes become more prevalent (Adames et al. 2019; Ahmed et al. 2021). This result is due to the assumptions that are built into the scale analysis. Second, the validity of the WTG equations hinge on the validity of Eq. (68), whose accuracy was not tested in this study. The moisture budget and parameterizations of convection and radiation become necessary when Eq. (68) is not an accurate approximation of the deviation of balance. Furthermore, the WTG equations are obtained as a result of scale analysis. While it is a useful starting point to understand atmospheric motions, it cannot account for the complex spatial and temporal interactions that occur in those motions, many which can render the WTG equations invalid. Last, we did not consider any potential for how the motions discussed here interact with the planetary boundary layer.

In conclusion, our results show that a variety of tropical motion systems exist. Many of these are in WTG balance. Furthermore, our results also underscore the importance of water vapor in the thermodynamics of tropical motions. It is important in six of the seven identified systems, and dominant in the two types of moisture modes that were identified. Additionally, nonlinear balance explains the part of the flow that deviates from strict WTG balance in the systems that are in WTG balance. The strictly WTG-balanced circulation and its deviation are tightly coupled and influence each other's evolution, as shown in Eq. (74). These results agree with and extend the findings Raymond et al. (2015) and Sessions et al. (2019) on the importance of balanced dynamics in the tropics to the case in which χ_w and ψ are of comparable magnitude. A better understanding of these interactions may lead to improved tropical weather forecasting, and a better representation of tropical motions in GCMs.

Acknowledgments. This work was partially motivated by discussions with Larissa Back, Angela Rowe, and Hannah Zanowski that arose from the master's defense of a graduate student of the author. The author thanks Adam Sobel and two anonymous reviewers for comments that greatly improved the contents of the manuscript. The author also thanks Víctor C. Mayta for suggesting the creation of Fig. 9. This work was partially funded by the National Science Foundation's Grant AGS-1841559 and the University of Wisconsin's startup package.

Data availability statement. No data were generated in this study.

REFERENCES

Adames, Á. F., and D. Kim, 2016: The MJO as a dispersive, convectively coupled moisture wave: Theory and observations. *J. Atmos. Sci.*, **73**, 913–941, https://doi.org/10.1175/JAS-D-15-0170.1.

——, and Y. Ming, 2018: Moisture and moist static energy budgets of South Asian monsoon low pressure systems in GFDL AM4.0. *J. Atmos. Sci.*, **75**, 2107–2123, https://doi.org/10.1175/JAS-D-17-0309.1.

——, and E. D. Maloney, 2021: Moisture mode theory's contribution to advances in our understanding of the Madden-Julian oscillation and other tropical disturbances. *Curr. Climate Change Rep.*, **7**, 72–85, https://doi.org/10.1007/s40641-021-00172-4.

——, D. Kim, S. K. Clark, Y. Ming, and K. Inoue, 2019: Scale analysis of moist thermodynamics in a simple model and the relationship between moisture modes and gravity waves. *J. Atmos. Sci.*, **76**, 3863–3881, https://doi.org/10.1175/JAS-D-19-0121.1.

——, ——, E. D. Maloney, and A. H. Sobel, 2020: The moisture mode framework of the Madden–Julian oscillation. *The Multiscale Global Monsoon System*, World Scientific, 273–287.

——, S. W. Powell, F. Ahmed, V. C. Mayta, and J. D. Neelin, 2021: Tropical precipitation evolution in a buoyancy-budget framework. *J. Atmos. Sci.*, **78**, 509–528, https://doi.org/10.1175/JAS-D-20-0074.1.

Ahmed, F., J. D. Neelin, and Á. F. Adames, 2021: Quasi-equilibrium and weak temperature gradient balances in an equatorial beta-plane model. *J. Atmos. Sci.*, **78**, 209–227, https://doi.org/10.1175/JAS-D-20-0184.1.

Benedict, J. J., and D. A. Randall, 2007: Observed characteristics of the MJO relative to maximum rainfall. *J. Atmos. Sci.*, **64**, 2332–2354, https://doi.org/10.1175/JAS3968.1.

——, E. D. Maloney, A. H. Sobel, and D. M. W. Frierson, 2014: Gross moist stability and MJO simulation skill in three full-

physics GCMs. *J. Atmos. Sci.*, **71**, 3327–3349, https://doi.org/10.1175/JAS-D-13-0240.1.

Bolin, B., 1955: Numerical forecasting with the barotropic model 1. *Tellus*, **7**, 27–49, https://doi.org/10.3402/tellusa.v7i1.8770.

Bretherton, C. S., and P. K. Smolarkiewicz, 1989: Gravity waves, compensating subsidence and detrainment around cumulus clouds. *J. Atmos. Sci.*, **46**, 740–759, https://doi.org/10.1175/1520-0469(1989)046<0740:GWCSAD>2.0.CO;2.

——, and A. H. Sobel, 2002: A simple model of a convectively coupled Walker circulation using the weak temperature gradient approximation. *J. Climate*, **15**, 2907–2920, https://doi.org/10.1175/1520-0442(2002)015<2907:ASMOAC>2.0.CO;2.

——, M. E. Peters, and L. E. Back, 2004: Relationships between water vapor path and precipitation over the tropical oceans. *J. Climate*, **17**, 1517–1528, https://doi.org/10.1175/1520-0442(2004)017<1517:RBWVPA>2.0.CO;2.

Browning, G., H. Kreiss, and W. Schubert, 2000: The role of gravity waves in slowly varying in time tropospheric motions near the equator. *J. Atmos. Sci.*, **57**, 4008–4019, https://doi.org/10.1175/1520-0469(2001)058<4008:TROGWI>2.0.CO;2.

Burpee, R. W., 1974: Characteristics of North African easterly waves during the summers of 1968 and 1969. *J. Atmos. Sci.*, **31**, 1556–1570, https://doi.org/10.1175/1520-0469(1974)031<1556:CONAEW>2.0.CO;2.

Charney, J. G., 1955: The use of the primitive equations of motion in numerical prediction. *Tellus*, **7**, 22–26, https://doi.org/10.3402/tellusa.v7i1.8772.

——, 1963: A note on large-scale motions in the tropics. *J. Atmos. Sci.*, **20**, 607–609, https://doi.org/10.1175/1520-0469(1963)020<0607:ANOLSM>2.0.CO;2.

Chikira, M., 2014: Eastward-propagating intraseasonal oscillation represented by Chikira–Sugiyama cumulus parameterization. Part II: Understanding moisture variation under weak temperature gradient balance. *J. Atmos. Sci.*, **71**, 615–639, https://doi.org/10.1175/JAS-D-13-038.1.

Clark, S. K., Y. Ming, and Á. F. Adames, 2020: Monsoon low pressure system–like variability in an idealized moist model. *J. Climate*, **33**, 2051–2074, https://doi.org/10.1175/JCLI-D-19-0289.1.

Daleu, C. L., and Coauthors, 2015: Intercomparison of methods of coupling between convection and large-scale circulation: 1. Comparison over uniform surface conditions. *J. Adv. Model. Earth Syst.*, **7**, 1576–1601, https://doi.org/10.1002/2015MS000468.

Delayen, K., and J.-I. Yano, 2008: Is asymptotic non-divergence of the large-scale tropical atmosphere consistent with equatorial wave theories? *Tellus*, **61A**, 491–497, https://doi.org/10.1111/j.1600-0870.2009.00404.x.

Diaz, M., and A. Aiyyer, 2013: Energy dispersion in African easterly waves. *J. Atmos. Sci.*, **70**, 130–145, https://doi.org/10.1175/JAS-D-12-019.1.

——, and W. R. Boos, 2021: Evolution of idealized vortices in monsoon-like shears: Application to monsoon depressions. *J. Atmos. Sci.*, **78**, 1207–1225, https://doi.org/10.1175/JAS-D-20-0286.1.

Emanuel, K. A., 1986: An air–sea interaction theory for tropical cyclones. Part I: Steady-state maintenance. *J. Atmos. Sci.*, **43**, 585–605, https://doi.org/10.1175/1520-0469(1986)043<0585:AASITF>2.0.CO;2.

——, 2020: Slow modes of the equatorial waveguide. *J. Atmos. Sci.*, **77**, 1575–1582, https://doi.org/10.1175/JAS-D-19-0281.1.

——, J. D. Neelin, and C. S. Bretherton, 1994: On large-scale circulations in convecting atmospheres. *Quart. J. Roy. Meteor. Soc.*, **120**, 1111–1143, https://doi.org/10.1002/qj.49712051902.

Ferreira, R. N., and W. H. Schubert, 1999: The role of tropical cyclones in the formation of tropical upper-tropospheric troughs. *J. Atmos. Sci.*, **56**, 2891–2907, https://doi.org/10.1175/1520-0469(1999)056<2891:TROTCI>2.0.CO;2.

Frierson, D. M. W., 2007: Convectively coupled Kelvin waves in an idealized moist general circulation model. *J. Atmos. Sci.*, **64**, 2076–2090, https://doi.org/10.1175/JAS3945.1.

Fuchs, Ž., and D. J. Raymond, 2002: Large-scale modes of a nonrotating atmosphere with water vapor and cloud–radiation feedbacks. *J. Atmos. Sci.*, **59**, 1669–1679, https://doi.org/10.1175/1520-0469(2002)059<1669:LSMOAN>2.0.CO;2.

——, and ——, 2017: A simple model of intraseasonal oscillations. *J. Adv. Model. Earth Syst.*, **9**, 1195–1211, https://doi.org/10.1002/2017MS000963.

——, ——, and S. Sentic, 2019: A simple model of convectively coupled equatorial Rossby waves. *J. Adv. Model. Earth Syst.*, **11**, 173–184, https://doi.org/10.1029/2018MS001433.

Gjorgjievska, S., and D. Raymond, 2014: Interaction between dynamics and thermodynamics during tropical cyclogenesis. *Atmos. Chem. Phys.*, **14**, 3065–3082, https://doi.org/10.5194/acp-14-3065-2014.

Gonzalez, A. O., and X. Jiang, 2019: Distinct propagation characteristics of intraseasonal variability over the tropical west Pacific. *J. Geophys. Res. Atmos.*, **124**, 5332–5351, https://doi.org/10.1029/2018JD029884.

Grise, K. M., and D. W. Thompson, 2012: Equatorial planetary waves and their signature in atmospheric variability. *J. Atmos. Sci.*, **69**, 857–874, https://doi.org/10.1175/JAS-D-11-0123.1.

Haertel, P. T., and G. N. Kiladis, 2004: Dynamics of 2-day equatorial waves. *J. Atmos. Sci.*, **61**, 2707–2721, https://doi.org/10.1175/JAS3352.1.

Haynes, P. H., and M. E. McIntyre, 1987: On the evolution of vorticity and potential vorticity in the presence of diabatic heating and frictional or other forces. *J. Atmos. Sci.*, **44**, 828–841, https://doi.org/10.1175/1520-0469(1987)044<0828:OTEOVA>2.0.CO;2.

——, and ——, 1990: On the conservation and impermeability theorems for potential vorticity. *J. Atmos. Sci.*, **47**, 2021–2031, https://doi.org/10.1175/1520-0469(1990)047<2021:OTCAIT>2.0.CO;2.

Heckley, W. A., and A. E. Gill, 1984: Some simple analytical solutions to the problem of forced equatorial long waves. *Quart. J. Roy. Meteor. Soc.*, **110**, 203–217, https://doi.org/10.1002/qj.49711046314.

Held, I. M., and B. J. Hoskins, 1985: Large-scale eddies and the general circulation of the troposphere. *Adv. Geophys.*, **28**, 3–31, https://doi.org/10.1016/S0065-2687(08)60218-6.

Hendon, H. H., and M. C. Wheeler, 2008: Some space–time spectral analyses of tropical convection and planetary-scale waves. *J. Atmos. Sci.*, **65**, 2936–2948, https://doi.org/10.1175/2008JAS2675.1.

Herman, M. J., and D. J. Raymond, 2014: WTG cloud modeling with spectral decomposition of heating. *J. Adv. Model. Earth Syst.*, **6**, 1121–1140, https://doi.org/10.1002/2014MS000359.

Holloway, C. E., and S. J. Woolnough, 2016: The sensitivity of convective aggregation to diabatic processes in idealized radiative-convective equilibrium simulations. *J. Adv. Model. Earth Syst.*, **8**, 166–195, https://doi.org/10.1002/2015MS000511.

Hoskins, B. J., I. N. James, and G. H. White, 1983: The shape, propagation and mean-flow interaction of large-scale weather systems. *J. Atmos. Sci.*, **40**, 1595–1612, https://doi.org/10.1175/1520-0469(1983)040<1595:TSPAMF>2.0.CO;2.

Houze, R. A., Jr., 2014: *Cloud Dynamics*. 2nd ed. International Geophysics Series, Vol. 104. Academic Press, 432 pp.

Inoue, K., and L. E. Back, 2015: Gross moist stability assessment during TOGA COARE: Various interpretations of gross moist stability. *J. Atmos. Sci.*, **72**, 4148–4166, https://doi.org/10.1175/JAS-D-15-0092.1.

——, and ——, 2017: Gross moist stability analysis: Assessment of satellite-based products in the GMS plane. *J. Atmos. Sci.*, **74**, 1819–1837, https://doi.org/10.1175/JAS-D-16-0218.1.

——, Á. F. Adames, and K. Yasunaga, 2020: Vertical velocity profiles in convectively coupled equatorial waves and MJO: New diagnoses of vertical velocity profiles in the wavenumber–frequency domain. *J. Atmos. Sci.*, **77**, 2139–2162, https://doi.org/10.1175/JAS-D-19-0209.1.

——, M. Biasutti, and A. M. Fridlind, 2021: Evidence that horizontal moisture advection regulates the ubiquitous amplification of rainfall variability over tropical oceans. *J. Atmos. Sci.*, **78**, 529–547, https://doi.org/10.1175/JAS-D-20-0201.1.

Janiga, M. A., and C. Zhang, 2016: MJO moisture budget during DYNAMO in a cloud-resolving model. *J. Atmos. Sci.*, **73**, 2257–2278, https://doi.org/10.1175/JAS-D-14-0379.1.

Jiang, X., Á. F. Adames, M. Zhao, D. Waliser, and E. Maloney, 2018: A unified moisture mode framework for seasonality of the Madden–Julian oscillation. *J. Climate*, **31**, 4215–4224, https://doi.org/10.1175/JCLI-D-17-0671.1.

Kiladis, G. N., C. D. Thorncroft, and N. M. J. Hall, 2006: Three-dimensional structure and dynamics of African easterly waves. Part I: Observations. *J. Atmos. Sci.*, **63**, 2212–2230, https://doi.org/10.1175/JAS3741.1.

——, M. C. Wheeler, P. T. Haertel, K. H. Straub, and P. E. Roundy, 2009: Convectively coupled equatorial waves. *Rev. Geophys.*, **47**, RG2003, https://doi.org/10.1029/2008RG000266.

Kim, J.-E., and C. Zhang, 2021: Core dynamics of the MJO. *J. Atmos. Sci.*, **78**, 229–248, https://doi.org/10.1175/JAS-D-20-0193.1.

Kuang, Z., 2011: The wavelength dependence of the gross moist stability and the scale selection in the instability of column-integrated moist static energy. *J. Atmos. Sci.*, **68**, 61–74, https://doi.org/10.1175/2010JAS3591.1.

Lorenz, E. N., 1960: Energy and numerical weather prediction. *Tellus*, **12**, 364–373, https://doi.org/10.3402/tellusa.v12i4.9420.

Majda, A. J., and R. Klein, 2003: Systematic multiscale models for the tropics. *J. Atmos. Sci.*, **60**, 393–408, https://doi.org/10.1175/1520-0469(2003)060<0393:SMMFTT>2.0.CO;2.

Mapes, B. E., 2000: Convective inhibition, subgrid-scale triggering energy, and stratiform instability in a toy tropical wave model. *J. Atmos. Sci.*, **57**, 1515–1535, https://doi.org/10.1175/1520-0469(2000)057<1515:CISSTE>2.0.CO;2.

——, and R. A. Houze Jr., 1995: Diabatic divergence profiles in western Pacific mesoscale convective systems. *J. Atmos. Sci.*, **52**, 1807–1828, https://doi.org/10.1175/1520-0469(1995)052<1807:DDPIWP>2.0.CO;2.

Martin, Z., S. Wang, J. Nie, and A. Sobel, 2019: The impact of the QBO on MJO convection in cloud-resolving simulations. *J. Atmos. Sci.*, **76**, 669–688, https://doi.org/10.1175/JAS-D-18-0179.1.

Matsuno, T., 1966: Quasi-geostrophic motions in the equatorial area. *J. Meteor. Soc. Japan*, **44**, 25–43, https://doi.org/10.2151/jmsj1965.44.1_25.

Mayta, V. C., and Á. F. Adames, 2021: 2-day westward-propagating inertio-gravity waves during GoAmazon. *J. Atmos. Sci.*, **78**, 3727–3743, https://doi.org/10.1175/JAS-D-20-0358.1.

——, G. N. Kiladis, J. Dias, P. L. Silva Dias, and M. Gehne, 2021: Convectively coupled Kelvin waves over tropical South America. *J. Climate*, **34**, 6531–6547, https://doi.org/10.1175/JCLI-D-20-0662.1, in press.

——, Á. F. Adames, and F. Ahmed, 2022: Westward-propagating moisture mode over the tropical Western Hemisphere. *Geophys. Res. Lett.*, **49**, e2022GL097799, https://doi.org/10.1029/2022GL097799.

McBride, J. L., and W. M. Gray, 1980: Mass divergence in tropical weather systems paper II: Large-scale controls on convection. *Quart. J. Roy. Meteor. Soc.*, **106**, 517–538, https://doi.org/10.1002/qj.49710644909.

Neelin, J. D., and I. M. Held, 1987: Modeling tropical convergence based on the moist static energy budget. *Mon. Wea. Rev.*, **115**, 3–12, https://doi.org/10.1175/1520-0493(1987)115<0003:MTCBOT>2.0.CO;2.

Ogrosky, H. R., and S. N. Stechmann, 2015: Assessing the equatorial long-wave approximation: Asymptotics and observational data analysis. *J. Atmos. Sci.*, **72**, 4821–4843, https://doi.org/10.1175/JAS-D-15-0065.1.

Ooyama, K. V., 1982: Conceptual evolution of the theory and modeling of the tropical cyclone. *J. Meteor. Soc. Japan*, **60**, 369–380, https://doi.org/10.2151/jmsj1965.60.1_369.

Powell, S. W., 2017: Successive MJO propagation in MERRA-2 reanalysis. *Geophys. Res. Lett.*, **44**, 5178–5186, https://doi.org/10.1002/2017GL073399.

Raymond, D. J., 1992: Nonlinear balance and potential-vorticity thinking at large Rossby number. *Quart. J. Roy. Meteor. Soc.*, **118**, 987–1015, https://doi.org/10.1002/qj.49711850708.

——, 2001: A new model of the Madden–Julian oscillation. *J. Atmos. Sci.*, **58**, 2807–2819, https://doi.org/10.1175/1520-0469(2001)058<2807:ANMOTM>2.0.CO;2.

——, and X. Zeng, 2005: Modelling tropical atmospheric convection in the context of the weak temperature gradient approximation. *Quart. J. Roy. Meteor. Soc.*, **131**, 1301–1320, https://doi.org/10.1256/qj.03.97.

——, and S. L. Sessions, 2007: Evolution of convection during tropical cyclogenesis. *Geophys. Res. Lett.*, **34**, L06811, https://doi.org/10.1029/2006GL028607.

——, and Ž. Fuchs, 2009: Moisture modes and the Madden–Julian oscillation. *J. Climate*, **22**, 3031–3046, https://doi.org/10.1175/2008JCLI2739.1.

——, and M. J. Herman, 2011: Convective quasi-equilibrium reconsidered. *J. Adv. Model. Earth Syst.*, **3**, M08003, https://doi.org/10.1029/2011MS000079.

——, S. L. Sessions, and Ž. Fuchs, 2007: A theory for the spinup of tropical depressions. *Quart. J. Roy. Meteor. Soc.*, **133**, 1743–1754, https://doi.org/10.1002/qj.125.

——, ——, A. H. Sobel, and Ž. Fuchs, 2009: The mechanics of gross moist stability. *J. Adv. Model. Earth Syst.*, **1** (3), https://doi.org/10.3894/JAMES.2009.1.9.

——, Ž. Fuchs, S. Gjorgjievska, and S. Sessions, 2015: Balanced dynamics and convection in the tropical troposphere. *J. Adv. Model. Earth Syst.*, **7**, 1093–1116, https://doi.org/10.1002/2015MS000467.

Roundy, P. E., and W. M. Frank, 2004: A climatology of waves in the equatorial region. *J. Atmos. Sci.*, **61**, 2105–2132, https://doi.org/10.1175/1520-0469(2004)061<2105:ACOWIT>2.0.CO;2.

Ruppert, J. H., and C. Hohenegger, 2018: Diurnal circulation adjustment and organized deep convection. *J. Climate*, **31**, 4899–4916, https://doi.org/10.1175/JCLI-D-17-0693.1.

Rushley, S. S., D. Kim, C. S. Bretherton, and M.-S. Ahn, 2018: Reexamining the nonlinear moisture-precipitation relationship over

the tropical oceans. *Geophys. Res. Lett.*, **45**, 1133–1140, https://doi.org/10.1002/2017GL076296.

Rydbeck, A. V., and E. D. Maloney, 2015: On the convective coupling and moisture organization of east Pacific easterly waves. *J. Atmos. Sci.*, **72**, 3850–3870, https://doi.org/10.1175/JAS-D-15-0056.1.

Sadler, J. C., 1976: A role of the tropical upper tropospheric trough in early season typhoon development. *Mon. Wea. Rev.*, **104**, 1266–1278, https://doi.org/10.1175/1520-0493(1976)104<1266:AROTTU>2.0.CO;2.

Schubert, W. H., S. A. Hausman, M. Garcia, K. V. Ooyama, and H.-C. Kuo, 2001: Potential vorticity in a moist atmosphere. *J. Atmos. Sci.*, **58**, 3148–3157, https://doi.org/10.1175/1520-0469(2001)058<3148:PVIAMA>2.0.CO;2.

Seidel, S. D., and D. Yang, 2020: The lightness of water vapor helps to stabilize tropical climate. *Sci. Adv.*, **6**, eaba1951, https://doi.org/10.1126/sciadv.aba1951.

Serra, Y. L., G. N. Kiladis, and M. F. Cronin, 2008: Horizontal and vertical structure of easterly waves in the Pacific ITCZ. *J. Atmos. Sci.*, **65**, 1266–1284, https://doi.org/10.1175/2007JAS2341.1.

Sessions, S. L., S. Sugaya, D. J. Raymond, and A. H. Sobel, 2010: Multiple equilibria in a cloud-resolving model using the weak temperature gradient approximation. *J. Geophys. Res.*, **115**, D12110, https://doi.org/10.1029/2009JD013376.

——, M. J. Herman, and S. Sentic, 2015: Convective response to changes in the thermodynamic environment in idealized weak temperature gradient simulations. *J. Adv. Model. Earth Syst.*, **7**, 712–738, https://doi.org/10.1002/2015MS000446.

——, S. Sentic, and D. J. Raymond, 2019: Balanced dynamics and moisture quasi-equilibrium in DYNAMO convection. *J. Atmos. Sci.*, **76**, 2781–2799, https://doi.org/10.1175/JAS-D-18-0173.1.

Snide, C. E., Á. F. Adames, S. W. Powell, and V. C. Mayta, 2022: The role of large-scale moistening by adiabatic lifting in the Madden–Julian oscillation convective onset. *J. Climate*, **35**, 269–284, https://doi.org/10.1175/JCLI-D-21-0322.1.

Sobel, A. H., and C. S. Bretherton, 2000: Modeling tropical precipitation in a single column. *J. Climate*, **13**, 4378–4392, https://doi.org/10.1175/1520-0442(2000)013<4378:MTPIAS>2.0.CO;2.

——, and ——, 2003: Large-scale waves interacting with deep convection in idealized mesoscale model simulations. *Tellus*, **55A**, 45–60, https://doi.org/10.3402/tellusa.v55i1.12084.

——, and D. Kim, 2012: The MJO-Kelvin wave transition. *Geophys. Res. Lett.*, **39**, L20808, https://doi.org/10.1029/2012GL053380.

——, and E. Maloney, 2013: Moisture modes and the eastward propagation of the MJO. *J. Atmos. Sci.*, **70**, 187–192, https://doi.org/10.1175/JAS-D-12-0189.1.

——, J. Nilsson, and L. M. Polvani, 2001: The weak temperature gradient approximation and balanced tropical moisture waves. *J. Atmos. Sci.*, **58**, 3650–3665, https://doi.org/10.1175/1520-0469(2001)058<3650:TWTGAA>2.0.CO;2.

——, S. Wang, and D. Kim, 2014: Moist static energy budget of the MJO during DYNAMO. *J. Atmos. Sci.*, **71**, 4276–4291, https://doi.org/10.1175/JAS-D-14-0052.1.

Straub, K. H., and G. N. Kiladis, 2003: The observed structure of convectively coupled Kelvin waves: Comparison with simple models of coupled wave instability. *J. Atmos. Sci.*, **60**, 1655–1668, https://doi.org/10.1175/1520-0469(2003)060<1655:TOSOCC>2.0.CO;2.

Vallis, G. K., 2017: *Atmospheric and Oceanic Fluid Dynamics*. Vol. 2. Cambridge University Press, 946 pp.

Wang, S., and A. H. Sobel, 2011: Response of convection to relative sea surface temperature: Cloud-resolving simulations in two and three dimensions. *J. Geophys. Res.*, **116**, D11119, https://doi.org/10.1029/2010JD015347.

——, ——, and Z. Kuang, 2013: Cloud-resolving simulation of TOGA-COARE using parameterized large-scale dynamics. *J. Geophys. Res. Atmos.*, **118**, 6290–6301, https://doi.org/10.1002/jgrd.50510.

——, ——, and J. Nie, 2016: Modeling the MJO in a cloud-resolving model with parameterized large-scale dynamics: Vertical structure, radiation, and horizontal advection of dry air. *J. Adv. Model. Earth Syst.*, **8**, 121–139, https://doi.org/10.1002/2015MS000529.

Wheeler, M., and G. N. Kiladis, 1999: Convectively coupled equatorial waves: Analysis of clouds and temperature in the wavenumber–frequency domain. *J. Atmos. Sci.*, **56**, 374–399, https://doi.org/10.1175/1520-0469(1999)056<0374:CCEWAO>2.0.CO;2.

——, ——, and P. J. Webster, 2000: Large-scale dynamical fields associated with convectively coupled equatorial waves. *J. Atmos. Sci.*, **57**, 613–640, https://doi.org/10.1175/1520-0469(2000)057<0613:LSDFAW>2.0.CO;2.

Wolding, B. O., E. D. Maloney, and M. Branson, 2016: Vertically resolved weak temperature gradient analysis of the Madden–Julian oscillation in SP-CESM. *J. Adv. Model. Earth Syst.*, **8**, 1586–1619, https://doi.org/10.1002/2016MS000724.

——, J. Dias, G. Kiladis, F. Ahmed, S. W. Powell, E. Maloney, and M. Branson, 2020: Interactions between moisture and tropical convection. Part I: The coevolution of moisture and convection. *J. Atmos. Sci.*, **77**, 1783–1799, https://doi.org/10.1175/JAS-D-19-0225.1.

Yano, J.-I., and M. Bonazzola, 2009: Scale analysis for large-scale tropical atmospheric dynamics. *J. Atmos. Sci.*, **66**, 159–172, https://doi.org/10.1175/2008JAS2687.1.

Yasunaga, K., and B. Mapes, 2012: Differences between more divergent and more rotational types of convectively coupled equatorial waves. Part I: Space–time spectral analyses. *J. Atmos. Sci.*, **69**, 3–16, https://doi.org/10.1175/JAS-D-11-033.1.

Yu, J.-Y., and J. D. Neelin, 1994: Modes of tropical variability under convective adjustment and the Madden–Julian oscillation. Part II: Numerical results. *J. Atmos. Sci.*, **51**, 1895–1914, https://doi.org/10.1175/1520-0469(1994)051<1895:MOTVUC>2.0.CO;2.